Mantle refertilization and magmatism in old orogenic regions: The role of late-orogenic pyroxenites

Lydéric France, Gilles Chazot, Jacques Kornprobst, Luigi Dallai, Riccardo Vannucci, Michel Grégoire, Hervé Bertrand, Pierre Boivin

Mantle refertilization and magmatism in old orogenic regions: The role of late-orogenic pyroxenites

Lydéric FRANCE[1*], Gilles CHAZOT[2,3], Jacques KORNPROBST[4], Luigi DALLAI[5], Riccardo VANNUCCI[6], Michel GREGOIRE[7], Hervé BERTRAND[8], Pierre BOIVIN[4,9, 10]

1: CRPG, UMR 7358, CNRS, Université de Lorraine, Vandœuvre-lès-Nancy, France

2: Université Européenne de Bretagne, France

3: Université de Brest ; CNRS ; UMR 6538 Domaines Océaniques; Institut Universitaire Européen de la Mer, Place Copernic, 29280 Plouzané, France

4: Clermont Université, Université Blaise Pascal, Laboratoire Magmas et Volcans, BP 10448, F-63000 Clermont-Ferrand, France

5: Istituto di Geoscienze e Georisorse (IGG), CNR, via Moruzzi 1, 56124 Pisa, Italia

6: Dipartimento di Scienze della Terra, Università di Pavia, via Ferrata 1, 27100 Pavia, Italia

7: Géosciences Environnement Toulouse, (GET, UMR 5563), Observatoire Midi-Pyrénées, 14 avenue E. Belin, 31400 Toulouse, France

8: Laboratoire de Géologie de Lyon, UMR-CNRS 5570, ENS Lyon et Université Lyon1, 46 Allée d'Italie, 69364 Lyon cedex 07, France

9: CNRS, UMR 6524, LMV, F-63038 Clermont-Ferrand, France

10: IRD, R 163, LMV, F-63038 Clermont-Ferrand, France

*****Corresponding author: lyde@crpg.cnrs-nancy.fr

Keywords: pyroxenite, mantle, cumulate, xenolith, metamorphic petrology, garnet, oxygen isotopes, eclogite, sapphirine, P-T conditions, Morocco, Jordan, Cameroon, French Massif-Central

Abstract

Pyroxenites and garnet pyroxenites are mantle heterogeneities characterized by a lower solidus temperature than the enclosing peridotites; it follows that they are preferentially involved during magma genesis. Constraining their origin, composition, and the interactions they underwent during their subsequent evolution is therefore essential to discuss the sources of magmatism in a given area. Pyroxenites could represent either recycling of crustal rocks in mantle domains or mantle originated rocks (formed either by olivine consuming melt-rock reactions or by crystal fractionation). Petrological and geochemical (major and trace elements, Sr-Nd and O isotopes) features of xenoliths from various occurrences (French Massif-Central, Jordan, Morocco and Cameroon) show that these samples represent cumulates crystallized during melt percolation at mantle conditions. They formed in mantle domains at pressures of 1-2 GPa during post-collisional magmatism (possibly Hercynian for the French Massif-Central, and Panafrican for Morocco, Jordan and Cameroon). The thermal re-equilibration of lithospheric domains, typical of the late orogenic exhumation stages, is also recorded by the samples. Most of the samples display a metasomatic overprint that may be either inherited or likely linked to the recent volcanic activity that occurred in the investigated regions.

The crystallization of pyroxenites during late orogenic events has implications for the subsequent evolution of the mantle domains. The presence of large amounts of mantle pyroxenites in old orogenic regions indeed imparts peculiar physical and chemical characteristics to these domains. Among others, the global solidus temperature of the whole lithospheric domain will be lowered; in turn, this implies that old orogenic regions are refertilized zones where magmatic activity would be enhanced.

1. Introduction

The shallowest part of the Earth's upper mantle is made primarily of peridotite, with spinel lherzolite and harzburgite being the most abundant lithologies. Pyroxenites and eclogites represent less than two percent of the upper mantle according to estimations based on isotopic considerations (Pertermann and Hirschmann, 2003), or up to five percent considering estimations made in orogenic peridotite massifs (e.g., Kornprobst, 1969; Pearson et al., 1993). Although they represent only a small volume of the upper mantle, pyroxenites and eclogites provide important information about dynamic processes occurring since the formation of the Earth, and about crustal recycling and melt circulation through the mantle (e.g., Downes, 2007; Gonzaga et al., 2010a). Due to their fertile composition and low solidus temperature compared to the host mantle peridotites, pyroxenites are quite relevant during mantle partial melting and basaltic magma genesis (Hirschmann and Stolper, 1996; Lambart et al., 2009). Their role in basalt genesis has indeed been inferred in oceanic and continental settings (e.g., Sobolev et al., 2005; Heinonen et al., 2013).

The origin of pyroxenites (as well as eclogites) found in mantle bodies or in mantle xenoliths is highly debated. They can represent dehydrated or residual and partially molten crustal lithologies recycled into the upper mantle through subduction zones (e.g., Allègre and Turcotte, 1986; Viljoen et al., 2005; Gonzaga et al., 2010a; Montanini et al., 2012). Such mantle heterogeneities usually display a greater variability in chemical and isotopic compositions compared to peridotitic mantle (e.g., Gonzaga et al., 2010a, b). Pyroxenites can also represent high-pressure cumulates fractionated from basaltic magmas circulating through the upper mantle (O'Hara and Yoder, 1967; Viljoen et al., 2005; Downes, 2007; Gonzaga et al., 2010a; Perinelli et al., 2011), creating a veined mantle below ancient magmatic provinces. Alternatively, this veined mantle has been interpreted as representing a lithospheric

refertilization stage resulting from olivine-melt consuming and clinopyroxene-orthopyroxene forming reactions (e.g., Bodinier et al., 2008).

The terminology in use (eclogite *versus* garnet pyroxenite) is mainly governed by the origin of these rocks. In their review on eclogites and garnet pyroxenites, Gonzaga et al. (2010a) related garnet pyroxenites to high-pressure mantle fractionation processes, and eclogites to recycling of crustal protoliths. Historically, eclogites have been defined as rocks containing pyrope-garnet and omphacitic-clinopyroxenes (Haüy, 1822). Moreover, eclogites differ from garnet pyroxenites in that they are more common in cratonic xenolith suites and have a higher jadeite component in clinopyroxenes (Pearson et al., 2005). Despite these differences, multidisciplinary studies are still necessary to decipher the origin of a given sample, and giving an *a priori* name is therefore hazardous. Hereafter, we will use the petrological term garnet pyroxenite (garnet when more than 10% garnet is present, and pyroxenite when olivine / [olivine+pyroxenes] < 40%, following the Streckeisen classification; Streckeisen, 1976).

The mineral assemblages developed in pyroxenites in response to changes in pressure and temperature conditions are of great help in reconstructing the evolutionary stages they underwent in the appropriate geodynamic setting (e.g., Montanini et al., 2006), whereas their chemical and isotopic compositions can be used to decipher their origin and evaluate their potential implication in magma genesis. The absence of modal olivine in mantle pyroxenites is associated with the presence of garnet under spinel lherzolite stability conditions (Kornprobst, 1969); this leads to the existence of two subfacies, namely the Seiland at lower and the Ariegite at higher pressure conditions (O'Hara, 1967). In these two subfacies, the Al-bearing phases consist of plagioclase and/or spinel, and spinel and/or garnet, respectively. These two subfacies subdivide the spinel lherzolite domain and allow us to determine more precisely the pressure-temperature-time (P-T-t) evolution of the lithosphere than with peridotitic samples.

We present here a petrological and geochemical study of 16 mantle garnet pyroxenite xenoliths (from Morocco, Jordan, Cameroon and France) that represent the rare material available for petro-geochemical studies. The aims of this study are: (i) to evaluate the similarities and/or differences between pyroxenite samples from the different regions; (ii) to constrain the origin of the studied pyroxenites; (iii) to constrain the P-T-t evolution of the studied pyroxenites within the mantle; (iv) to evaluate the relations between the determined P-T-t paths and the geodynamic history of the regional lithosphere; and (v) to discuss the influence of these mantle heterogeneities on the subsequent evolution of the lithosphere.

2. Regional settings and sampling localities

In order to compare the geodynamic evolution and chemical and isotopic composition of pyroxenites, we studied samples from four localities, each with different geodynamic histories: the French Massif Central (Europe), Morocco and Cameroon (Africa) and Jordan (on the Arabian plate; Fig. 1).

French Massif Central (FMC): The Massif Central (Fig. 1a) represents one of the biggest parts of the Variscan belt of Western Europe. Alkaline volcanism developed throughout Cenozoic times, with the last manifestation occurring in the Chaîne des Puys 6,900 ± 110 yr. cal. as the lake Pavin maar (Juvigné et al., 1996). The origin of this volcanism is still debated, and is either attributed to the presence of a thermal anomaly related to a mantle plume (e.g., Granet et al., 1995) or to asthenospheric upwelling related to the nearby Alpine orogeny (Merle and Michon, 2001).

Mantle xenoliths are present in several locations of the FMC. Two distinct domains, probably inherited from Hercynian times, are recognized N and S of an E-W line located ~45°30'N (Lenoir et al., 2000). Both domains have been variously depleted through melting ~360 Ma ago, and have been enriched by metasomatic fluids (carbonatitic to the North, and rather

related to silicate-melts to the South; Wittig et al., 2007) likely related to the Cenozoic plume (Zangana et al., 1997; Wittig et al., 2007).

Three of the studied samples come from the Devès volcanic field (S domain; LN-78 and LP-27 from Le Marais de Limagne, and SD-53 from Saint-Didier d'Allier), a basaltic plateau emplaced between 2.7 and 0.6 Ma (Nehlig et al., 2001). Teleseismic tomography studies indicate that the thermal anomaly in the mantle between 100 and 140 km below the Devès area is the largest of the FMC (Sobolev et al., 1996). One sample comes from Le Pouget, near Montpellier; this locality does not belong to the FMC but, instead, to the 'pyreneo-corso-sarde' Alpine belt. As the basement of this orogenic segment is also made of old Hercynian lithosphere, the Le Pouget sample will be described together with the FMC samples. This last sample has been briefly studied in previous works (Babkine et al., 1968; Fabriès et al., 1987).

Cameroon (Fig. 1b): The oldest Cameroon terrains were structured during Eburnean times some 2.1 Ga ago and were reworked during the Panafrican orogeny (Castaing et al., 1994). Many granite bodies were emplaced around 520 Ma (Lassere et al., 1981).

Pyroxenites were sampled in the Youkou maar, in the Adamaoua volcanic plateau (Temdjim, 2006). This maar belongs to the Cameroon Volcanic Line (CVL; part of a still-active fault belt in West Africa), which is characterized by important Tertiary and Quaternary alkaline magmatism extending off-continent to several oceanic islands. Volcanism in this area started around 60 Ma ago (Cantagrel et al., 1978) and is still active today. Mantle xenoliths (spinel lherzolites being the most common) are present in volcanic rocks from both oceanic and continental parts of the CVL. Several studies have emphasized a partial melting event probably related to late Proterozoic crust formation (Lee et al., 1996). In many places, the mantle rocks show evidence of interaction with enriched partial melts, probably related to the Mesozoic breakup of Pangaea and the emplacement of the St. Helena mantle plume (Lee et al., 1996; Caldeira and Munha, 2002; Temdjim et al., 2004).

Morocco (Fig. 1c): The middle Atlas area of Morocco is part of the Atlas Mountain range of North Africa and was mainly structured during the Panafrican orogeny, lasting roughly from 700 to 530 Ma (Gasquet et al., 2005). The orogenic period was followed by the formation of large Paleozoic sedimentary basins that were strongly folded during late Carboniferous–Permian compression (Pique and Michard, 1989). Cenozoic volcanism started before 35 Ma; the last eruptions are probably not older than 0.5 Ma (El Azzouzi et al., 2010) and are tentatively linked to a hot line spreading from the Siroua to Oujda (e.g., El Azzouzi et al., 2010).

Mantle xenoliths are present in volcanic rocks from the middle Atlas, and show a wide range of lithological and chemical heterogeneity. As in Cameroon, an older melting event is recorded by the chemistry of clinopyroxene (Raffone et al., 2009; Wittig et al., 2010). In most samples, this event has been overprinted by a widespread modal metasomatism (Pezzali et al., 2015). This metasomatic episode is probably very young (less than 200 Ma) and involves the percolation of alkaline melts with HIMU affinity as well as carbonatitic fluids (Raffone et al., 2009; Natali et al., 2013; Pezzali et al., 2015).

The Morocco samples come from the Bou-Ibalratene basaltic maar belonging to a volcanic group of nearly 100 monogenic edifices oriented about N170°E, and located South of Azrou in the middle Atlas.

Jordan (Fig. 1d): Jordan is located in the northern part of the Arabian-Nubian shield and was affected by important metamorphism and magmatism during the Panafrican orogeny from 640 to 540 Ma ago (Stein and Goldstein, 1996). Large alkaline volcanic fields named ‘Harrats’ are present all along the Arabian plate from Yemen in the South to Jordan and Syria in the North. They are related to the Red Sea and Jordan rifts and were emplaced during Tertiary and Quaternary times (Bertrand et al., 2003).

The Jordan samples come from three different maars belonging to the large, NW-SE trending, Harrat Ash Shaam that extends from SW Syria to the Northern part of Saudi Arabia. Studies concerning Harrat Ash Shaam mantle xenoliths have shown that the mantle in this region was affected by partial melting and refertilization events between 870 and 620 Ma ago. These processes are related to the formation of juvenile crust in a continental arc system (Krienitz and Haase, 2011).

3. Analytical techniques

This study is based on major and trace element and isotope analyses of whole rocks and mineral separates (separated under binocular microscope for their purity after crushing, sieving and washing). In-situ chemical analyses have been made on polished thin sections (30, 100 or 150 µm thick). Details on analytical techniques and settings are given in supplementary material.

4. Petrology

4.1. Petrography

The sample labels, rock types and modes of the studied samples, and the abbreviations used for minerals are presented in Table 1.

Pyroxenites from the FMC have recrystallized granoblastic textures with average grain size of 1 mm for the samples from the Devès volcanic province (LN-78, LP-27 and SD-53); grain size is smaller in the sample from Le Pouget (pyroxenes ~0.25 mm, Spl and Grt ~0.75 mm). The prevailing mineral assemblage in all the samples is Cpx+Grt+Opx+Spl±Am. Grt is often located around green Spl and contains green Spl, Pl, Opx and Cpx inclusions that are surrounded by radial fractures (Fig. 2a-b). Those inclusions are remnants of a former paragenesis. In LN-78 larger Cpx grains (>2 mm) display Opx exsolutions (Fig. 2c). This

198 sample is composite with an Am-free part and an Am-rich zone. In the three Devès samples,
199 small grains (50 – 100 µm) of Opx, Pl and brownish Spl are locally observed at the contact
200 between Grt and Cpx (Fig. 2d). In all samples, Grt is surrounded by a thin (5 to 40 µm; Fig.
201 2b, d) brownish kelyphite rim made of Opx-Pl-Spl (proportions 64:23:13%, respectively,
202 estimated using mineral compositions and the method of France and Nicollet, 2010).
203 Samples TAK-3 and TAK-4 from Morocco have a granular texture with an average grain size
204 of 3 mm and show a penetrative foliation. The paragenesis is Grt+Opx+Cpx+Spl for TAK-3
205 and Grt+Cpx+Spl+Spr+Opx for TAK-4. In TAK-3, Grt occurs around the Spl demonstrating
206 an earlier crystallization of Spl, whereas in TAK-4, the Grt-Spl association is observed only
207 locally (Fig. 2e-f). In TAK-3 large Cpx grains (6 mm) contain Grt and Opx exsolutions, and
208 some very thin (1-2 µm) Spl exsolutions are observed in other Cpx. In TAK-4, Spr is present
209 as inclusions in Spl or Cpx, surrounding the Spl at the Grt contact (Fig. 2e-f), or as thin
210 exsolutions in Cpx. In this same sample a peculiar inclusion is observed in a Cpx grain,
211 containing a Spl+Spr+Pl+Opx assemblage (Fig. 2g). Both samples suffered extended Grt
212 kelyphitization (~0.4 mm large in average).
213 Petrographically, the Cameroon samples can be divided in two groups. The first group (YK-
214 01, YK-05 and YK-16) represents initial Cpx megacrysts (0.5-3cm) that exsolve Grt grains up
215 to 500 µm wide (Fig. 2h-j). In YK-01 Cpx encloses Spl grains that are surrounded by
216 abundant Grt (Fig. 2h). YK-05 megacrysts record a deformation stage and exsolve Opx (Fig.
217 2i-j). The second group (YK-03, YK-12, YK-13) is characterized by a polycrystalline
218 Cpx+Opx+Grt+Spl assemblage (average grain size 3 mm). In these samples, Grt is either
219 exsolved from Cpx, or localized around Cpx grains and concentrated at the Spl rim. In YK-13,
220 Opx is also localized around Cpx grains and is probably exsolved. In this sample, some
221 apatite is observed, locally included in Grt or Opx. Thin Am exsolutions (~20 µm wide) are
222 also observed in some Cpx grains. In Cpx from all Cameroon samples, very thin (1-2 µm

wide) Spl exsolutions are present; in samples YK-13 and YK-16, these can reach tens of µm and are locally surrounded by Grt exsolutions. Am is present in all the samples except YK-01. A thin (≤ 20 µm) kelyphitization zone is present around Grt, and a melting zone (< 15 µm) is often observed at the contact between kelyphite and surrounding minerals. Later surface processes are documented by some carbonate veins that crosscut Grt kelyphite and melting zones.

The Jordan samples include Spl Grt pyroxenites (JO-7b and JO-7h) and Grt free orthopyroxenites (JO-10e and JO-12h); JO-12h is an Am-bearing olivine orthopyroxenite. The average grain size in all samples is 1 mm (Fig. 2k). In JO-7b and JO-7h, Grt (~50 µm) is exsolved from pyroxene, around which it concentrates; some Grt also appears around green (in JO-7b, Fig. 2k) or brown (in JO-7h) Spl. In JO-7h some very thin (~2 µm) Spl exsolutions are observed in Cpx. In JO-10e orthopyroxenite, rutile is observed along two exsolution directions in Opx (Fig. 2l); moreover, this sample is diffusely permeated by dikelets and pockets of carbonate. In JO-7h, Opx is fractured and oxidized at its rim. In both JO-7b and JO-7h, Grt is kelyphitized (~40 µm wide) at the margins.

4.2. Major element mineral chemistry

Mineral compositions are very homogeneous in each studied sample, allowing us to use average compositions to compare the different samples (Table 2). Cpx and Opx are diopside and enstatite, respectively. Their compositions are broadly similar in the samples from the different provenances (Fig. 3a). In Cpx, wollastonite content is higher than 43%, ferrosilite content lower that 10%, and jadeite content varies from 4.7 to 12.5%, whereas in Opx wollastonite content is lower than 2%, ferrosilite content varies between 9 and 18%, and jadeite content is below 1%. TAK-4 Cpx are not stoichiometric; they are silica (Si/(Ca+Na+Mg+Fe)=1.04) and Ca (X_{Wo}=0.51) enriched. Grt are pyrope (Fig. 3b), with

compositions between 62 and 73% for the pyrope component (Mg) and between 11 and 24% for the almandine component (Fe) at a nearly constant grossular (Ca) content (~13%). Spl show a wide range of compositions. The Cr_2O_3 vs. Al_2O_3 anti-correlation (R^2=0.96) is related to the Al-Cr substitution in Spl and shows a variation from 0 to 30% of the chromite component. For all the studied samples, the ratio *Mg-component/Fe^{2+}-component* (*spinel s.s./hercynite*) is around 2, and #Cr varies from 1 to 12% in all samples except JO-12h, for which the value is 30.5% (with #Cr=Cr/(Cr+Al) in molar proportions). For the samples displaying two Spl generations (LN-78, LP-27 and SD-53), the brown ones (second generation) are poorer in chromite component than the primary green ones. Pl compositions are variable, ranging from andesine in FMC samples (with anorthite content varying from 35 to 47 mol%), to bytownite in TAK-4 (Morocco; An_{84}). Analyzed amphiboles are magnesiohastingsites in LN-78, YK-05 and YK-13, pargasites in YK-03 and ferro-edenite in JO-12h. Olivine is Fo_{89} in JO-12h.

5. Mineral trace element compositions

Trace element compositions of minerals have been obtained for Cpx and Grt in all samples, and for Am, Pl, and Opx when these minerals were large enough (Table 3). Cpx trace element composition is variable in the different samples, and sometimes within a single sample. In FMC samples (Fig. 4a), the Cpx show variable light-rare earth elements (LREE) contents, ranging from strongly depleted (in Le Pouget sample) to slightly enriched compared to the medium-REE (MREE). They are also depleted in heavy-REE (HREE), reflecting their chemical equilibrium with Grt (see section 8.1.2 “Cpx/Opx and Cpx/Grt partition coefficients”). In sample LN78, some Cpx located close to Am grains are highly enriched in LREE, less HREE depleted than other Cpx, and have REE content similar to associated Am grains. In the two Morocco samples (Fig. 4a), the Cpx have REE normalized contents that

decrease from the LREE to the HREE region. In TAK-4 the decrease from the LREE to the HREE is more pronounced than in TAK-3 and slight positive Eu and Sr anomalies are present (Fig. 4b). Similar to their analogues from FMC, Cpx in the Cameroon samples are all HREE depleted (Fig. 4c), in agreement with the presence of Grt. Their LREE composition is variable and ranges from 0.6 to more than 10 times the chondrite value. Grt-bearing samples from Jordan show two types of Cpx compositions (Fig. 4c); Cpx grains in contact with Grt are strongly depleted in HREE relative to MREE, whereas those far from Grt are only slightly depleted. Their LREE content is also variable, from largely depleted in JO-7b to slightly enriched in JO-7h. In Grt-free samples, Cpx possess higher REE abundances and are LREE enriched. In all these samples, Cpx have very low Nb, Ta and often Zr and Hf contents (Fig. 4b, d). All the analyzed Grt grains show typical REE patterns, highly enriched in HREE (up to 100x chondrite in TAK-3 from Morocco) in comparison to largely depleted LREE contents (Fig. 4e). Some Grt display relatively flat patterns from MREE to HREE, reflecting the low HREE contents of the whole rock. Grt is strongly enriched in U (Fig. 4f). Pl in FMC samples is LREE enriched and shows strong Eu, Sr and Ba positive anomalies (Table 3).

6. Whole rock major and trace element compositions

Whole rock major element compositions are summarized in Table 4 and Figure 5. Mg# (where Mg# = Mg/(Mg+Fe) in molar proportions) varies from 79.8 in SD-54 (FMC) to 89.3 in JO-7h (Jordan; Table 4). SiO_2 content ranges from 42.6 to 54.7 wt%; the lowest values are found in the two samples from Morocco which are thus classified as ultramafic rocks while all other samples are mafic rocks (Le Bas and Streckeisen, 1991). MgO content varies from 15.5 wt% in LP-27 (FMC) to 33.1 wt% in JO-12h (Jordan). Al_2O_3 content ranges from 3.2 wt% in JO-10e (Jordan) to 22.5 wt% in TAK-4 (Morocco). CaO content varies from 1.7 wt% in JO-12h (Jordan) to 16.4 wt% in Le Pouget sample (FMC). FeO_t (all iron expressed as FeO)

content varies from 4.6 wt% in JO-7h (Jordan) to 8.1 wt% in JO-10e (Jordan). Na_2O content ranges from 0.04 wt% in JO-12h (Jordan) to 1.41 wt% in YK-13 (Cameroon). In all the oxide-oxide composition plots, whole rock compositions plot between the main bearing minerals, namely Cpx, Opx, Spl, and Grt. Some samples, especially those from Morocco, are furthermore slightly shifted toward the Spl and/or Spr composition. MgO is correlated with SiO_2, and anticorrelated with CaO and Al_2O_3. The average composition of primitive MORB and alkaline melts are added in Figure 5, and are considered as possible proxies of a prospective trapped melt in mantle domains.

Whole rock trace element concentrations are summarized in Table 4 and Figure 6. Whole rock REE content for FMC pyroxenites show typical spoon-shaped patterns with high HREE content, depletion in MREE and enrichment in LREE (Fig. 6a). The two different parts of LN-78 have parallel REE patterns, the Am-rich part being more LREE enriched; Le Pouget sample possesses similar MREE and HREE composition, but is largely depleted in LREE, with La lower than 0.1x chondrite, in agreement with its strongly LREE depleted Cpx (Fig. 4a). The two samples from Morocco have contrasting REE compositions; TAK-3 pyroxenite shows a pattern similar to the FMC pyroxenites, whereas the Spr-bearing TAK-4 sample has a very low HREE content (< 3x chondrite) coupled with a marked LREE enrichment (La > 35x chondrite), and a small positive Eu anomaly associated with a positive Sr anomaly. Similar to the FMC samples, two types of REE patterns are displayed by the Cameroon pyroxenites (Fig. 6c); they all have low HREE content, and most of the samples are LREE depleted. Only two samples (YK-13 and YK-16) show LREE enrichment. The pyroxenites from Jordan also have contrasted REE patterns (Fig. 6e). Three samples are LREE enriched, with $(La/Yb)_n$ values ranging from 2.5 to 7 and quite variable HREE compositions, while sample JO-7b is LREE depleted.

In trace element spider diagrams (Fig. 6b, d, f), all samples present large negative Rb and Nb anomalies, associated with negative Zr anomalies (except for TAK-3 that displays a slight positive anomaly). Most of the samples also display a positive Sr anomaly; only JO-10e (Jordan) displays a negative Sr anomaly.

7. Isotopic data

Sr-Nd isotope data have been obtained on separated Cpx from four samples from Jordan, three from Cameroon, and two from Morocco (Table 5; not enough material was available for other samples). $^{87}Sr/^{86}Sr$ values are homogeneous and range from 0.702661 to 0.703375 (Fig. 7); in contrast, $^{143}Nd/^{144}Nd$ values are more variable and range between 0.512774 and 0.513433. Both the lowest and highest values are observed in Jordan samples. All the samples, except JO-7b and TAK-3, plot below the mantle array; most values are close to the HIMU component (Zindler et Hart, 1986).

50 analyses of oxygen isotopic ratios have been obtained on Cpx, Opx, Grt and Spl separates (Table 5). Most of the values fall within the mantle range for peridotites (Ionov et al., 1994; Mattey et al., 1994a; Chazot et al., 1997; Zhang et al., 2000), with $\delta^{18}O$ ranging from 4.82 to 5.72‰ for Cpx, from 4.94 to 6.12‰ for Opx, from 5.15 to 5.97‰ for Grt, and from 4.33 to 4.97‰ for Spl (Fig. 8). Fractionation between Grt and Cpx is positive and close to 0.3‰ with the exception of three samples from Cameroon having slightly negative fractionation values (Fig. S1a). Fractionation between Opx and Cpx is also positive (except for two samples, Fig. S1b), and in the range of values observed in mantle lherzolites from Yemen (Chazot et al., 1997).

8. Discussion

The various petrographical and geochemical data presented are discussed hereafter to determine the last equilibration stage conditions (T, fO_2, section 8.1) of the studied Grt pyroxenites, and to track their origin (recycled or not?, section 8.2) and the metasomatic reactions they subsequently suffered (section 8.3). Pyroxenite pressure-temperature variations through subsolidus evolution are reconstructed for each sample (section 8.4), and the apparent inter- and intra-region variability (petrographical and geochemical) are discussed in section 8.5. Finally we present our hypothesis in a geodynamic framework to discuss implications in terms of mantle refertilization (section 8.6).

8.1. Last equilibration stage conditions

8.1.1. Thermometry and oxybarometry

Equilibrium temperature (T) estimates are presented in Table 1. Opx-Cpx equilibrium T of Grt-bearing peridotites and pyroxenites are best estimated using the Taylor (1998) geothermometer (Wu and Zhao, 2012), and are as follows: 730°C and 930-1080°C (Le Pouget and other FMC samples, respectively), 910°C (TAK-3, Morocco), 780-810°C (Jordan), and 900-980°C (Cameroon). Equilibrium T cannot be estimated for TAK-4 since it contains aluminous diopside. For comparison, Opx-Grt equilibrium T, calculated using the Nimis and Grütter (2010) geothermometer, are as follows: 715-1020°C (FMC), 890°C (TAK-3, Morocco), 720-760°C (Jordan), and 870-980°C (Cameroon). In general, equilibrium T calculated with both geothermometers are consistent. Because 2+ cations diffuse faster than 3+ cations, T calculated using major element based thermometers are likely to be indicative of late stage equilibration T, whereas REE-in-two-pyroxene thermometers are expected to be indicative of sub-magmatic T (e.g., Liang et al., 2013). Valid results have been obtained using the Liang et al. (2013) model for two samples from the present study: LN-78: 1376 ±126 °C,

and LP-27: 1194 ±69 °C; those equilibrium T are consistent with the record of an early magmatic stage.

Redox conditions of mantle domains are usually estimated using oxybarometers that necessitate olivine bearing-rocks (e.g., Goncharov and Ionov, 2012), and are thus not appropriate for the olivine-free pyroxenites studied here. Fe^{3+} concentrations in Cpx, Opx, and Grt have been estimated using stoichiometric criteria following the classical approach of Droop (1987); corresponding $Fe^{3+}/\Sigma Fe$ values are reported in Table S1 and Fig. 9. Although such calculation results should be taken with caution, good correlations exist between $(Fe^{3+}/\Sigma Fe)_{Opx}$ and $(Fe^{3+}/\Sigma Fe)_{Cpx}$ (R^2=0.69), between $(Fe^{3+}/\Sigma Fe)_{Grt}$ and $(Fe^{3+}/\Sigma Fe)_{Opx}$ (R^2=0.85), and between $(Fe^{3+}/\Sigma Fe)_{Grt}$ and $(Fe^{3+}/\Sigma Fe)_{Cpx}$ (R^2=0.71; Fig. 9). Those good correlations strongly support the validity of the stoichiometric calculations for the present study: $(Fe^{3+}/\Sigma Fe)_{Cpx}$ ranges from 0 to 0.6, $(Fe^{3+}/\Sigma Fe)_{Opx}$ from 0 to 0.22, and $(Fe^{3+}/\Sigma Fe)_{Grt}$ from 0 to 0.21. $(Fe^{3+}/\Sigma Fe)_{Melt}$ was calculated using $(Fe^{3+}/\Sigma Fe)_{Cpx}$ values and the approach formulated in France et al. (2010). Rough estimates for ΔFMQ (Fayalite-Magnetite-Quartz oxygen fugacity buffer) were obtained using the correlation between ΔFMQ and $(Fe^{3+}/\Sigma Fe)_{Grt}$ presented by Goncharov and Ionov (2012). $(Fe^{3+}/\Sigma Fe)_{Melt}$ is plotted against ΔFMQ in Fig. 9.

More generally, the FMC samples appear to be the most reduced pyroxenites with $(Fe^{3+}/\Sigma Fe)_{Melt}$ ranging from 0.4 to 0.6; Jordan pyroxenites are slightly less reduced with an average $(Fe^{3+}/\Sigma Fe)_{Melt}$ of 0.6; the average $(Fe^{3+}/\Sigma Fe)_{Melt}$ for Morocco samples is 0.66; and Cameroon samples are the most oxidized samples studied herein with $(Fe^{3+}/\Sigma Fe)_{Melt}$ ranging from 0.56 to 0.83 for an average value of 0.73 (Fig. 9).

8.1.2. Cpx/Opx and Cpx/Grt partition coefficients

The major element compositional homogeneity of all the minerals among the studied samples, and the presence in most of the samples of well-developed exsolution lamellae indicate that

(at least partial) intra-sample equilibrium was achieved; this is supported by the typical mantle T calculated from the chemical composition of Cpx, Opx and Grt (Table 1). Oxygen isotope data also show that no large disequilibrium exists between minerals in the studied pyroxenites. This chemical equilibrium among minerals was also tested by trace element partition coefficient calculations between Cpx and Opx, and between Cpx and Grt in the different samples (Fig. 10). The calculated $\mathbf{K_{D(Cpx\text{-}Grt)}}$ values are in the range of values published by Viljoen et al. (2005) for group II eclogites from South Africa, interpreted as crystallization products of small-volume melts in the lithospheric mantle. Our values are also very similar to those obtained in a Cpx megacryst aggregate crystallized from a MORB type magma in the lithospheric mantle of China (Huang et al., 2007), and to $\mathbf{K_{D(Cpx\text{-}Grt)}}$ determined experimentally at pressures varying from 2 to 3 GPa (Johnson, 1994). $\mathbf{K_{D(Cpx\text{-}Grt)}}$ are dependent on the major element phase compositions (e.g., Harte and Kirkley, 1997); calculations accounting for mineral compositions align closely with $\mathbf{K_{D(Cpx\text{-}Grt)}}$ values obtained in the present study (Fig. 10). These results support that Cpx and Grt have attained chemical equilibrium at mantle conditions in all the studied samples before their fast transport to the surface. $\mathbf{K_{D(Cpx\text{-}Opx)}}$ values are compared to results obtained by Raffone et al. (2009) on lherzolites and harzburgites from Morocco (Fig. 10). Although a strong variability is observed in our data (due to large errors on the trace element concentrations of Opx that are strongly depleted in trace elements), $\mathbf{K_{D(Cpx\text{-}Opx)}}$ are in the range of mantle values determined by Raffone et al. (2009).

8.2. Pyroxenite origin as mantle cumulates

It is still a matter of debate whether pyroxenite xenoliths brought to the surface by volcanic processes represent metamorphically transformed crustal rocks (of either continental or oceanic origin) or are the final products of melt circulation, crystallization and evolution in the

mantle. Here we use highly detailed petrological observations and major and trace element compositions, coupled with stable and radiogenic isotopic compositions to decipher their origin.

8.2.1. Whole rock compositions as a proxy of initial cumulative assemblages

Whole rock major element compositions define relatively good correlations for SiO_2, CaO and Al_2O_3 versus MgO content (Fig. 5), and Al_2O_3 and SiO_2 are also well correlated. The pyroxenites studied here show an increase in SiO_2 content correlated to an increase in MgO (Fig. 11), which is in contrast to classic liquid lines of descent that highlight melt differentiation processes (e.g., for MORB, calc-alkaline, or alkaline rocks) characterized by a decrease in MgO when SiO_2 increases. High concentrations of highly compatible elements such as Ni can be used to identify cumulative rocks, in which their concentration is by definition higher than in the corresponding equilibrium melts. The Ni content of the studied pyroxenites (~300-900 ppm) is much higher than most primitive MORBs (~300 ppm, and decreasing with differentiation; Fig. 11), indicating that they cannot represent liquids, but rather are cumulates (either s.s. cumulates or cumulates resulting from percolative fractional crystallization). At this stage of discussion, their origin as crustal or mantle cumulates cannot be deciphered.

Since the studied pyroxenites represent cumulative rocks, their whole rock composition (major and trace elements) is indicative of the modal proportion of the initial cumulative assemblage; for example, the high Ni content attests to the presence of Spl among the cumulative minerals. We now present evidence supporting the assemblages that are reported in Table 1. The presence of magmatic Grt in four samples (FMC samples, and TAK-3 from Morocco; Fig. 6) is confirmed by the whole rock enrichment in HREE relative to MREE. The major element composition and Ni content of those samples also indicate that Cpx-Opx-Spl

were part of the initial cumulative assemblage (red dotted samples in Fig. 5). Among the studied pyroxenites, 3 samples from Cameroon (YK-01, YK-03, YK-12) display small but significant positive Eu anomalies (Fig. 6), classically indicating magmatic Pl. However, similar anomalies have been reported in spinel-bearing peridotitic Cameroon mantle, and attributed to regional metasomatism (e.g., Temdjim et al., 2004). This signature being regional, and in the absence of other evidence, we follow their interpretation and infer that Pl was not part of the initial cumulative assemblage in Cameroon samples. Only TAK-4 from Morocco displays coupled positive Eu and Sr anomalies (Fig. 6) that have not been reported for peridotitic samples from this area, and should be attributed to the presence of Pl in the initial cumulative assemblage. In this sample, the major element and Ni concentrations point to the additional presence of Cpx and Spl in the initial cumulative assemblage (Fig. 5). Major elements and Ni concentrations of Cameroon samples demonstrate that Cpx-Sp (±Opx) were part of the initial cumulative assemblage in all samples (Fig. 5), consistent with petrographic observations. Petrographic relations also suggest that apatite was present as a magmatic mineral in YK-13. According to petrography, major elements, and Ni contents, Opx was the main cumulative mineral in JO-10e and JO-12h, together with Ol-Spl-Cpx in JO-12h, and Spl-Cpx in JO-10e; two pyroxenes and Spl were present in the initial cumulative assemblages of JO-7b, and 7h (Fig. 5, Table 1).

In addition to the cumulative mineral record, Downes (2007) invoked a trapped melt component to account for the whole rock major element compositions of orogenic pyroxenites interpreted to be mantle cumulates. In order to test this hypothesis, the compositions of relatively primitive mantle melts (represented by primitive MORBs and alkaline basalts) have been added to all graphs of Fig. 5. Only two samples (LP-27 from FMC, and YK-13 from Cameroon) seem to record a slight influence of trapped melt in their whole rock composition, as highlighted by their high Na_2O contents. This hypothesis is consistent with the LREE

enrichment of those samples; in addition YK-13 is the only sample to contain early magmatic apatite, also consistent with a possible trapped melt component.

The initial cumulative assemblages determined here will be used in section 8.4 to determine the in which mantle domain crystallization occurred. Finally the major and trace element whole rock compositions of the studied cumulative pyroxenites are only representative of the initial cumulative assemblage (nature of the phases and modal composition) and are thus not indicative of the composition of the parental melts that thus cannot be determined.

An alternative hypothesis to the cumulative origin of the studied pyroxenites is that Grt-pyroxenites form as refractory residues after partial melting of eclogitic metagabbros (e.g., Montanini et al., 2012). However, residual Grt-pyroxenites are expected to preserve the initial Eu and Sr anomalies that are characteristic of eclogites with a recycled origin (Marchesi et al., 2013). In addition, we have identified that the initial cumulative assemblages are, depending on the studied pyroxenites, either Cpx-Opx-Grt-Spl or Cpx-Opx-Spl (±Pl, ±Ol, ±Ap; Table 1), which is not consistent with residual assemblages derived from either gabbroic protoliths (Montanini et al., 2012; Marchesi et al., 2013) or Pl-free pyroxenites or eclogites (Kogiso et al., 2003; Lambart et al., 2009). Such a model is therefore not valid for the pyroxenites studied here.

TAK-3 and TAK-4 Grt-bearing pyroxenites from Morocco are slightly off the general trends observed for major elements (Fig. 5). These samples are shifted toward Spl and/or Spr compositions in most oxide composition diagrams, suggesting that higher amounts of Spl and/or Spr were present as primary magmatic phases in these samples. The possibility that Spr is a liquidus phase in mafic to intermediate magmas at high pressure conditions (from 1.1 to 3 GPa) has been highlighted by Liu and Presnall (2000). However, these authors pointed out that Spr has rarely been described as a magmatic phase in natural rocks as it mostly occurs as a metamorphic mineral. Textural, petrological and geochemical evidence presented here does

not clarify an igneous or metamorphic origin of Spr; this will be further discussed in section 8.4 *'P-T-t path reconstructions'*.

In summary, the studied pyroxenites represent cumulative rocks that initially crystallized Cpx, Opx, and for some samples Grt and Spl (with trace apatite in one sample; Table 1); Pl was part of the initial cumulative assemblage in only one sample (TAK-4). Such cumulative assemblages are not expected in lower crustal (continental & oceanic) settings where Pl is usually the dominant phase. Additionally, Px±Spl±Grt cumulates are expected at shallow mantle depths according to experimental petrology constraints (e.g., Green & Ringwood, 1967), and are very commonly described among mantle xenoliths (e.g., Kaeser et al., 2009; Perinelli et al., 2011) or in orogenic ultramafic massifs (e.g., Downes, 2007). The likely mantle origin of the studied cumulates can be further tested using isotopic constraints.

8.2.2. Isotopic constraints support a mantle protolith

The oxygen isotopic composition of minerals is useful for constraining mantle versus recycled origins of pyroxenites and eclogites (e.g., Downes, 2007; Gonzaga et al., 2010a). Cpx, Grt, Opx, and Spl analyzed in this study have oxygen isotopic values typical of mantle minerals (4.8-6.1‰, Fig. 8; e.g., Mattey et al., 1994a; Chazot et al., 1997), in contrast to more variable compositions of Cpx and Grt in recycled eclogites (2-10‰; e.g., Mattey et al., 1994b; Gonzaga et al., 2010a) and bulk oceanic crust (3.7-13.6‰; e.g., Gregory and Taylor, 1981). Deep crustal portions of oceanic crust (primarily Pl-rich cumulates) may display typical mantle values (Gao et al., 2006), but are distinct due to strong Eu anomalies not observed in the pyroxenites studied herein. Major element compositions of the studied pyroxenites do not overlap the composition of neither volcanic, nor plutonic oceanic crust (Fig. 11), also strongly supporting that studied pyroxenites do not derive from recycled oceanic crust. It should be noted here that similar cumulative rocks have been recognized at Moho depth in the Kohistan

overthickened arc crust (35-45 km; Burg, 2011). The studied pyroxenites are therefore most likely mantle cumulates; only TAK-4, which displays mantle like $\delta^{18}O$ values and magmatic Pl, may represent either a shallow mantle or deep crustal cumulate. Inter-mineral $\delta^{18}O$ variations are presented in supplementary figure S1; as a whole they are consistent with a mantle origin.

Sr-Nd isotope data obtained on Cpx separates are used to test our previous conclusions. Garrido et al. (2000) showed that ~65% of the Sr concentration of an ultramafic rock, and ~15% of the Nd, is hosted in solid, melt, and fluid inclusions, as well as grain boundaries; Sr-Nd isotopic data obtained on Cpx separates (the main REE bearing mineral) should thus be preferred to whole rock measurements. As a whole, the studied pyroxenites have Sr and Nd isotopic ratios that are slightly above and below, respectively, the average DMM composition (Fig. 7), in contrast to recycled eclogites that display more heterogeneous values than the host mantle (Gonzaga et al., 2010a). Only two samples, TAK-3 and JO-7b (from Morocco and Jordan, respectively), have higher Nd isotope ratios compared to DMM. The Nd isotopic signature of JO-7b closely matches that of another garnet pyroxenite from Israel (BS-701 in Stein et al., 1993) and peridotite samples from Saudi Arabia (Henjes-Kunst et al., 1990; Blusztajn et al., 1995), and is probably a time integrated effect of a high Sm/Nd ratio (Sm/Nd = 0.566; e.g., Borghini et al., 2013), which is the highest among all the samples. TAK-3 from Morocco does not have a high Sm/Nd ratio, but its isotopic composition is very close to that of lherzolite and websterite samples analyzed in the same area (Raffone et al., 2009). Excluding TAK-3 and JO-7b, the Sr-Nd isotopic compositions of the studied pyroxenites, although heterogeneous, overlap those obtained on mantle rocks from the various areas considered (Fig. 7), as is expected for pyroxenites with origins as segregations from mantle melts (e.g., Downes, 2007; Gonzaga et al., 2010a).

Our findings are in agreement with numerous previous studies identifying mantle pyroxenites as mantle cumulates rather than the products of deep crustal recycling (O'Hara and Yoder, 1967; Frey, 1980; Downes, 2007; Griffin & O'Reilly, 2007; Perinelli et al., 2011). The opposing view that mantle heterogeneities originate mainly from recycling associated with subduction zones (Allègre and Turcotte, 1986) is not applicable to most of the studied samples.

8.3. Evidence for subsequent metasomatic interactions

Most of the studied pyroxenites show evidence of late melt percolation and cryptic and/or modal metasomatism. Two samples from Cameroon (YK-13 and YK-16) are LREE enriched and sample YK-05, although LREE depleted, shows a slight enrichment in La compared to Ce. These LREE enriched samples also have high concentrations in Ba, Sr, U and Th and low concentrations in Zr and Hf. This metasomatic signature has already been observed in spinel lherzolites from the Nyos volcano along the CVL (Temdjim et al., 2004), and is therefore a regional overprint. The Morocco pyroxenites are also enriched in LREE, Ba, U, Th and Sr, although more markedly in TAK-4 than in TAK-3. Raffone et al. (2009) documented similar enrichments in peridotite xenoliths from the same volcanic province and showed that they are related to alkaline melt percolation, probably associated with late Cretaceous or Eocene volcanism. A metasomatic overprint is also present in three of the four studied Jordan samples. Spidergrams highlight the LREE enrichment relative to MREE, and positive Ba, U, and Th anomalies that are similar to metasomatic enrichments previously described in Jordan lithospheric mantle, and possibly related to Pan-African subduction (Shaw et al., 2007). Metasomatism is also evident in the pyroxenites from the FMC. All the whole-rocks, except the southernmost sample (Le Pouget), have spoon-shaped REE patterns with decreasing REE content from Lu to Nd, and are enriched in LREE (La, Ce and Pr), clearly pointing to LREE

depleted protoliths, further enriched by LREE-rich percolating melts. These samples are also highly enriched in U and Th, and sometimes depleted in Nb, Zr and Hf.

LN-78 is a composite sample with an Am-bearing and an Am-free part. In the Am-bearing part, Cpx is more LREE-enriched, and is in chemical equilibrium with coexisting Am as attested by the $D_{REE}^{Cpx/Am} \approx 1$ (Chazot et al., 1996). In the Am-free part, Cpx has complex REE patterns with HREE decreasing from Eu to Lu due to preferential incorporation of these elements in coexisting Grt. Rare earths were initially decreasing from Eu to La (similar to Le Pouget sample), but La and Ce have been selectively enriched during melt percolation and crystallization of Am and Cpx in the Am-bearing part of the sample; similar conclusions have been proposed by Downes et al. (2003). Similar metasomatic overprints with LREE, U, and Th enrichments, and Zr-Hf and Nb-Ta depletions have been observed in peridotite xenoliths from different localities in the FMC (Lenoir et al., 2000, Féménias et al., 2003, Dautria et al., 2010); those overprints are ascribed for most of the elements to Variscan (or late Variscan) -- possibly subduction-related -- metasomatism (Lenoir et al., 2000; Féménias et al., 2003). Other authors link this metasomatic event to the arrival of a mantle plume head in the early Cenozoic (Dautria et al., 2010). Some xenoliths originated in the southern part of the FMC do not show any metasomatic overprint (Dautria et al., 2010), in agreement with the lack of enrichment in the Le Pouget sample.

A metasomatic overprint may be hard to distinguish from a trapped melt component present in the initial cumulative assemblage. Na content may be used as it is not expected to be particularly enriched by metasomatic fluid percolation in comparison to other major elements, however it is useful to track a trapped melt component in cumulates (see section 8.2.1, and Fig. 5). Among the studied samples only LP-27, and YK-13 have been shown to record a trapped melt component; all trace element characteristics discussed above for the other samples are likely related to metasomatic enrichments.

As discussed in Pezzali et al. (2015), the samples displaying the weakest metasomatic overprint can be considered as geochemical remnants of the pre-metasomatic lithospheric mantle. Those are Le Pouget sample for FMC lithospheric mantle, Jo-7b for Jordan lithospheric mantle, YK-01, and YK-12 for Cameroon lithospheric mantle.

8.4. P-T-t path reconstructions and pyroxenite evolution within mantle domains

Various geochemical data presented here have highlighted an origin as mantle fractionated melts for the studied samples. Precise petrological observations and whole rock trace element contents are here used to constrain the P evolution of these cumulates and to reconstruct the corresponding P-T-t paths. To proceed, the P-T stability fields, the associated facies and subfacies, and the corresponding subsolidus reactions separating lithospheric mantle domains, documented in Fig. 12a, will be considered. Initial cumulative assemblages, and the sequence of subfacies crossed during the P-T-t evolution are recalled in Table 1.

FMC pyroxenites display recrystallized textures resulting from various sub-solidus mineral reactions. Grt entered the mineral assemblage as a liquidus phase (section 8.2), consistent with a first crystallization of the FMC pyroxenites in the Ariegite subfacies (Fig. 12b). However the numerous inclusions (green Spl, Cpx, Opx and Pl; Fig. 2a-b) observed in Grt show that the present-day Ariegite-subfacies mineral assemblage (Cpx+Grt+Opx+Spl±Am) does not represent that of the initial cumulate, but rather derivates from metamorphic reactions. This mineral assemblage preserved as inclusions in Grt thus testifies for an early Seiland pyroxenite facies assemblage. Some large Cpx grains (up to 2 mm) containing Opx exsolutions (Fig. 2c) have escaped the general recrystallization process and are still reminiscent of an early cooling. A demixing T of ~1275°C is estimated for sample LN-78 using image processing, mineral compositions, and Carlson and Lindsley (1988) relations. In all the FMC samples but Le Pouget pyroxenite, Grt grains in contact with Cpx grains undergo

a later reaction leading to the local development of Pl, Opx and brown Spl (Fig. 12b), marking the return of the samples into the Seiland P-T domain. P-T-t paths for FMC samples are therefore summarized as follows (Fig. 12b): samples crystallized in Ariegite subfacies conditions (magmatic Grt), suffered an early T decrease (large Cpx grains with Opx exsolutions), and then underwent a concomitant P and T decrease that allowed a transition towards the Seiland subfacies (testified by Opx-Spl-Pl inclusions in present-day Grt); a further decrease in T brought the samples back into the Ariegite domain crystallizing the present-day Grt that contains relics of the former Seiland stage (Opx-Spl-Pl in Grt). A final decompression (or reheating) event that once again shifted some samples into the Seiland stability field.

A similar approach is followed to reconstruct the P-T-t evolution of the Morocco samples (Fig. 12c). Grt was a liquidus phase in TAK-3 (Ariegite facies conditions; section 8.2) but was absent when TAK-4 crystallized at a shallower depth. TAK-3 also contains some large Cpx grains with Opx exsolutions, indicating a T decrease after crystallization. Grt currently present in TAK-3 are mainly located around Spl (Fig. 2e-f) and formed by the reaction Opx+Spl+Pl->Grt+Cpx that documents the transition from the Seiland to the Ariegite subfacies (a previous transition from the Ariegite facies crystallization conditions to the Seiland subfacies is not documented by the mineralogy). Although TAK-4 did not crystallize in Ariegite facies conditions (no liquidus Grt, but magmatic Pl), abundant and large Grt and Cpx grains associated with the absence of Ol provide evidence of subsolidus equilibration under those conditions. The presence of a small Spr rim between Spl and Grt (Fig. 2e-f) suggests that the transition from Seiland to Ariegite subfacies conditions was mainly governed by a decrease in T inducing the reaction Opx+Spl+Pl->Grt+Spr; this is consistent with the Al-rich composition of TAK-4 Opx that is required for such a reaction (France et al., 2009). Alternatively, if TAK-4 was crystallized at deep crustal levels (see section 8.2.2), the cooling stage associated with this reaction may have been associated with a pressure increase. We will hereafter consider

only the less complex model that necessitates only a cooling stage. The presence of numerous Spr inclusions in Spl (Fig. 2e-f) and of one Spr relic surrounded by small crystals of Opx, Spl and Pl within a Cpx grain (Fig. 2a) document a further reaction, namely Grt+Spr->Opx+Spl+Pl, before the sample equilibrated in the Ariegite subfacies. This reaction marks the transition from the Spr-bearing Ariegite subfacies to the Spr-absent Ariegite subfacies, probably in response to a decrease in P. Despite those P-T-t estimates, Spr-bearing TAK-4 appears to have a rather complex paragenesis evolution. Further constraints from thermodynamic models will be needed to decipher a more precise evolution, however such work is beyond the scope of the present study. P-T-t paths for Morocco pyroxenites are therefore mostly characterized by a cooling event subsequent to crystallization that it is possibly followed by a concomitant P and T decrease before re-equilibration at lower T.

Pyroxenites from Cameroon contain large amounts of Cpx that exsolves Grt and sometimes Opx. Grt was not a liquidus phase when these cumulates crystallized, as shown by their relatively flat whole rock REE patterns (Fig. 6), constraining their formation in the Seiland subfacies (Fig. 12b). As previously discussed for the FMC and Morocco samples, exsolution of Opx is related to a decrease in T after crystallization. The occurrence of Grt is also related to a strong cooling event when it exsolved from Cpx or crystallized around Spl while the samples were moved to the Ariegite facies. This evolution can be accounted for by an isobaric T decrease or a concomitant T and P decrease. P-T-t paths for Cameroon pyroxenites therefore record a rather simple P-T-t trajectory marked mainly by a decrease in T (Fig. 12b). Evolution in pressure is poorly constrained, and a slight decompression may have occurred.

Pyroxenites from Jordan show only limited mineralogical reactions that can be used to decipher their P-T-t evolution (Fig. 12c). Pyroxenes from JO-12h are the most magnesian among the studied samples, Spl contains the highest amount of Cr_2O_3, and ~10% Ol is present; altogether those observations point to a parental melt that was slightly more primitive

than for other samples. In this pyroxenite, the absence of Pl and the presence of Ol+Cpx+Opx+Spl indicates that the reaction separating the Seiland subfacies and the Pl-lherzolite facies (Cpx+Opx+Spl->Ol+Pl) has not occurred. JO-12h therefore equilibrated in the Seiland subfacies. Grt was not a liquidus phase in any of the Jordan samples (Fig. 6; section 8.2), also implying crystallization in the Seiland subfacies. When present, Grt appears as exsolutions in pyroxene or around Spl (JO-7b and JO-7h), and so is clearly a subsolidus mineral. Grt exsolutions in pyroxenes are also indicative of a marked cooling event from the Seiland to the Ariegite field. Also consistent with an important cooling event are the numerous rutile exsolution lamellae in Opx of JO-10e (Fig. 2l). Indeed during crystallization at high pressure, in the absence of Ol and Spl, Ti is accommodated by Opx, and can be exsolved to form rutile exsolution needles during cooling (Verhoogen, 1962; Moore, 1968). P-T-t paths of Jordan samples are therefore mainly governed by a strong temperature decrease but are not well constrained in pressure (Fig. 12c). As is the case for Cameroon samples, a slight decrease in pressure may have occurred during thermal equilibration toward cooler conditions (Fig. 12c).

8.5. Inter- and intra-sites variability

Invoking a common cumulative process for the formation of the studied pyroxenites may sound odd given the inter- and intra-region petrographical and geochemical variability of the samples. Nevertheless, partial crystallization of mantle derived melts during interactions with peridotites at various depths has the potential to crystallize such apparently heterogeneous cumulates (Downes, 2007). In particular, whole rock compositions (major and trace elements) are only representative of the initial cumulative assemblage (± metasomatism) that has been sampled by a given xenolith (Fig. 13). An extreme case would be that a small size xenolith might sample only one mineral of this initial cumulative assemblage (e.g., Cpx, Opx, Grt, Spl;

694 cases 1, 2, 3 in Fig. 13). A more likely case would be that a xenolith samples a poly-mineral
695 piece of the initial cumulative assemblage (cases 4, 5 in Fig. 13). In that case, the whole rock
696 composition represents a mixing of the mineral compositions that relies on the modal
697 proportion within the initial cumulative assemblage (Fig. 13b-c). One striking feature is that
698 the modal composition of a given xenolith does not represent the modal proportion of the
699 initial cumulative assemblage as cumulates have suffered several metamorphic reactions
700 during their subsolidus evolution (Fig. 12, 13). The present day modal composition of a given
701 sample is therefore not directly representative of the whole rock composition (e.g., TAK-4
702 contains 56 % Grt when the trace element content shows that Grt was not part of the initial
703 cumulative assemblage). The widespread metasomatic events that have affected most of the
704 samples are expected to modify mainly the trace element budgets (e.g., LREE enrichments;
705 samples 1, 2, 4, 5 in Fig. 13c).
706 Given the various crystallization pressures (Seiland versus Ariegites subfacies; Table 1), the
707 numerous initial modal proportions that a given xenolith may sample (Fig. 13), and the range
708 of metasomatic enrichments that can affect the samples (Fig. 13c, and section 8.3), it is likely
709 that the samples display a strong inter- and intra-region variability, though they share a
710 common genesis.
711

712 **8.6. Geodynamic implications**

713 **8.6.1. Late-orogenic genesis of pyroxenites**

714 Petrological and geochemical evidences reported above, highlight that all the studied
715 pyroxenite xenoliths are products of melt crystallization at mantle conditions (1-2 GPa).
716 Similar cumulative rocks to those studied here have been recognized at Moho depth in
717 overthickened arc crust (Burg, 2011) where they crystallized prior to the thinning and
718 exhumation of the thickened crust. Cumulates have later undergone subsolidus evolution

719 under progressively changing P and T conditions; reconstructed P-T-t paths therefore also
720 highlight the P-T-t evolution of the regional host mantle, and can be used to discuss the
721 geodynamic settings that resulted in pyroxenite crystallization. Two P-T-t path types are
722 observed among the samples: the first is characterized by a strong cooling event that may have
723 been accompanied by a pressure decrease (Cameroon and Jordan samples; Fig. 12), and the
724 second is characterized by two important cooling stages separated by a period during which P
725 and T decrease jointly (FMC and Morocco samples; Fig. 12). The four studied areas have
726 been implicated in orogenic episodes in the last 800 Ma (either Panafrican or Hercynian). In
727 this perspective, the crystallization of mantle melts at depth, followed by a strong decrease in
728 T, and then by a decompression stage, can only occur during the exhumation of an orogenic
729 domain, and the associated thermal re-equilibration. Similar P-T paths for mantle rocks have
730 been described in different areas (Müntener, 1997; Fabriès et al., 1998; Kaeser et al., 2009),
731 and major magmatic episodes (e.g., magmatic underplating) are well known to occur in the
732 late evolution of orogenic domains (e.g., Henk et al., 1997; Fabriès et al., 1998; Cottin et al.,
733 1998; Féménias et al., 2003; Kaeser et al., 2009; McCarthy and Müntener, 2015). Along with
734 underplating occurring at Moho depth, large circulations of melts in deeper mantle domains
735 are expected and associated with refertilization reactions (e.g., McCarthy and Müntener,
736 2015). The melting event may start during the first stage of exhumation when mantle is
737 upwelling roughly adiabatically (isostatic re-equilibration). Post-crystallization equilibration
738 to the local geothermal T is recorded by the first part of the cooling stage. Following
739 crystallization and cooling, Morocco and FMC (and possibly Cameroon and Jordan) samples
740 underwent decompression tentatively related to the continuation of erosion and tectonic
741 collapse of the orogenic edifices. All the studied cumulates record the late orogenic stage
742 corresponding to the thermal re-equilibration along the continental geotherm (last cooling
743 stage). FMC samples from the Devès volcanic field have recorded a late P decrease; this event

744 could be linked to the Cenozoic bulging affecting the FMC (e.g., Sobolev et al., 1996;
745 Seranne, 1999). This is consistent with the absence of this last P drop in the southernmost
746 sample (Le Pouget), as no bulging has been described in the southern part of the FMC (e.g.,
747 Sobolev et al., 1996; Seranne, 1999).

748 The late-orogenic origin of the studied cumulates can be challenged by chronological
749 constraints; indeed Nd isotopic compositions can be used to put some constraints on the
750 timing of these events (e.g., Bizimis et al., 2005). Although these estimates should be
751 considered with serious caution (e.g., Wittig et al., 2006; Downes, 2007), building time
752 estimates using Nd in Cpx seems appropriate as those minerals host ~80% of the whole rock
753 Nd budget (Garrido et al., 2000). Assuming that in each region the pyroxenites formed from a
754 similar melt with homogeneous isotopic composition, samples from Cameroon have
755 crystallized between 700 and 1000 Ma ago. Such an estimation is valid for Jordan
756 pyroxenites, for which the origin can be estimated between 550 and 650 Ma. Morocco
757 samples are strongly overprinted by metasomatic circulations, and although time estimates are
758 consistent with late Panafrican orogeny (~520 Ma), those samples will not be considered here.
759 For Cameroon and Jordan, these rough time estimates correspond, with large uncertainties, to
760 the main Panafrican orogenic events affecting the crust and the upper mantle in these areas.
761 Again, these time constraints should be considered with serious caution as most of the
762 samples have been affected by post-crystallization metasomatism, which may have modified
763 Sm/Nd ratios and Nd isotopic compositions.

764 As a whole, the pyroxenites were formed in mantle conditions during late-orogenic
765 magmatism associated with orogenic exhumation (Fig. 14a-c). The recorded orogenic cycle is
766 probably the last main one in each region, and may be Panafrican for Jordan, Morocco and
767 Cameroon, and Hercynian for FMC. During their subsequent evolution, cumulates have
768 suffered several interactions with percolating fluids and melts.

769

770 **8.6.2. Mantle refertilization and forthcoming magma genesis**

771 We have shown that the studied Grt pyroxenites are mantle cumulates that crystallized during
772 the relaxation following orogenic events, and subsequently underwent modal and cryptic
773 metasomatism. Pyroxenites are fertile lithologies as their solidus is crossed at lower T than the
774 lherzolite solidus; up to 15% pyroxenite partial melting can be reached before the onset of
775 lherzolite melting (Hirschmann and Stolper, 1996). The addition of a pyroxenite component in
776 a given mantle domain consequently corresponds to a refertilization stage (e.g., Bodinier et
777 al., 2008), and the presence of pyroxenitic and metasomatic lithologies in the mantle has
778 strong implications on basalt genesis (either MORB or OIB; Allègre and Turcotte, 1986;
779 Hirschmann and Stolper, 1996; Hirschmann et al., 2003; Kogiso et al., 2003; Kogiso et al.,
780 2004; Pilet et al., 2008). The present study thus highlights that a refertilization stage of
781 lithospheric mantle can occur during the late orogenic re-equilibration period. It follows that
782 subsequent magmatic activity can be enhanced in old orogenic regions (such as FMC,
783 Morocco, Cameroon, Jordan), as it can be initiated earlier, and may be characterized by higher
784 magma volumes than in a non-affected region (Fig. 14). Nevertheless, tracking the implication
785 of such fertile lithologies in recent volcanism remains elusive as the melt-peridotite reactions
786 that occurred during melt ascent prevent the geochemical tracking of this influence (e.g., Le
787 Roux et al., 2009; Lambart et al., 2009).

788

789 **9. Conclusions**

790 The petrographical, geochemical, and isotopic study of garnet bearing pyroxenite xenoliths
791 from four localities (FMC, Morocco, Jordan and Cameroon) allows characterization of their
792 genesis and subsequent evolution. The whole-rock major element compositions and
793 compatible element abundances, the absence of Pl in the initial cumulative assemblage for all

the samples (but one sample from Morocco), and mineral oxygen isotopic compositions highlight a cumulative mantle origin. Metamorphic reactions, exsolutions and trace element whole-rock concentrations demonstrate that crystallization pressures ranged between 1 and 2 GPa (30-60 km depth) depending on the samples. P-T-t paths based on well characterized petrographical relations and calculated equilibrium temperatures attest to important movements in the respective lithospheres, whereas the presence of some hydrous minerals such as amphiboles, and incompatible element concentrations attest to a metasomatic overprint in most of the samples; this metasomatic enrichment also affects the host mantle. In their geodynamical context, the samples are interpreted as representing the crystallization of percolating melts formed at mantle conditions during exhumation of orogenic domains. Although variable due to the long-term integration of various father/daughter ratios, the Sr and Nd isotope signatures are consistent with crystallization during Panafrican times for Cameroon, Morocco and Jordan samples.

The results presented here highlight that exhumation of orogenic domains and the associated sub-adiabatic decompression trigger mantle partial melting; the melt percolating the mantle crystallizes, at least partially, to form the studied cumulative pyroxenites. At mantle conditions, pyroxenites are low melting point lithologies; their crystallization in mantle domains therefore implies its refertilization. As a consequence, the magmatism in old orogenic regions such as FMC, Morocco, Cameroon and Jordan, will be enhanced, and old orogenic domains would be precursor zones for magmatism that would be initiated earlier and would be volumetrically larger than in non-affected areas.

Acknowledgments

We express our warm thanks to the various people involved at different technical stages of this work: C. Bosq, and D. Auclair-Aubierge for assistance during sample preparation, and

TIMS measurements; J.L. Devidal for assistance during EPMA measurements; and J.L. Piro for assistance during LA-ICP-MS measurements. H. Downes, M. Wilson, and B. Ildefonse are thanked for useful comments on an early version of the manuscript. Two anonymous reviewers, Guilio Borghini, and the associate Editor are thanked for their constructive comments that have helped to largely improve the manuscript. C. Cordier is thanked for valuable discussions, and for her help for illustrations. We also thank J.C. Vilminot and D. Velde, who provided us garnet pyroxenite samples from the Devès Massif, together with related valuable geochemical data, J.P. Lorand for providing us Le Pouget sample from the MNHN-Paris collection, and R. Temdjim who shares the Cameroon samples property with P. Boivin. This is CRPG contribution n°XXXX.

References

Allègre, C.J., Turcotte, D.L., 1986. Implications of a two-component marble-cake mantle. Nature 323, 123-127.

Anders, E., Grevesse, N., 1989. Abundances of elements: Meteoritic and solar. Geochimica et Cosmochimina Acta 53, 197-214.

Babkine, J., Conquere, F., Vilminot, J., 1968. Découverte d'une enclave d'ariégite à grenat dans l'absarokite du Pouget (Herault). Comptes Rendus de l'Académie des Sciences 267, 1266-1269.

Baker, J., Chazot, G., Menzies, M., Thirlwall M., 1998. Metasomatism of the shallow mantle beneath Yemen by the Afar Plume—Implications for mantle plumes, flood volcanism, and intraplate volcanism. Geology 26, 431-434. doi:10.1130/0091-7613(1998)026<0431:MOTSMB>2.3.CO;2.

Ballentine, C.J., Lee, D.C., Halliday, A.N., 1997. Hafnium isotopic studies of the Cameroon line and new HIMU paradoxes. Chemical Geology 139, 111-124.

Bertrand, H., Chazot, G., Blichert-Toft, J., Thoral, S., 2003. Implications of widespread HIMU volcanism on the Arabian Plate for the composition of the Afar mantle plume and lithoshere. Chemical Geology 198, 47-61.

Bizimis, M., Sen, G., Salters, V.J.M., Keshav, S., 2005. Hf-Nd-Sr isotope systematics of garnet pyroxenites from salt lake crater, Oahu, Hawaii: Evidence for a depleted component in Hawaiian volcanism. Geochimica et Cosmochimina Acta 69-10, 2629-2646.

Blusztajn, J., Hart, S.R., Shimizu, N., McGuire, A.V., 1995. Trace-element and isotopic characteristics of spinel peridotite xenoliths from Saudi Arabia. Chemical Geology 123, 53-65.

Bodinier, J.L., Garrido, C.J., Chanefo, I., Bruguier, O., Gervilla, F., 2008. Origin of Pyroxenite-Peridotite Veined Mantle by Refertilization Reactions: Evidence from the Ronda Peridotite (Southern Spain). Journal of Petrology 49(5), 999-1025. doi: 10.1093/petrology/egn014.

Borghini, G., Rampone, E., Zanetti, A., Class, C., Cipriani, A., Hofmann, A.W., Goldstein, S.L., 2013. Meter-scale Nd isotopic heterogeneity in pyroxenite-bearing Ligurian peridotites encompasses global-scale upper mantle variability. Geology 41-10, 1055-1058.

Burg, J.P., 2011. The Asia-Kohistan-India collision: Review and discussion. In: Arc-continent collision. Brown, D., Ryan, P.D., (*Editors*), Springer-Verlag, Berlin, 279-309, *http://dx.doi.org/10.1007/978-3-540-88558-0*

Caldeira, R., Munha, J.M., 2002. Petrology of ultramafic nodules from São Tomé Island, Cameroon Volcanic Line (oceanic sector). Journal of African Earth Sciences 34, 231-246.

860 Cantagrel, J.M., Jamond, C., Lassere, M., 1978. Le magmatisme alcalin de la Ligne du Cameroun au Tertiaire
861 inférieur, données géochronologiques K/Ar. C. R. Somm. Soc. Géol. France 6, 300-303.
862 Carlson, W.D., Lindsley, D.H., 1988. Thermochemistry of pyroxenes on the join $Mg_2Si_2O_6$-$CaMgSi_2O_6$.
863 American Mineralogist 73, 242-252.
864 Castaing, C., Feybesse, J.L., Thiéblemont, D., Triboulet, C., Chèvremont, P., 1994. Palaeogeographical
865 reconstructions of the Pan-African/Brasiliano orogen: closure of an oceanic domain or intracontinental
866 convergence between major blocks? Precambrian Research 69, 327-344.
867 Chazot, G., Menzies, M.A., Harte, B., 1996. Determination of partition coefficients between apatite,
868 clinopyroxene, amphibole and melt in natural spinel lherzolites from Yemen: Implications for wet
869 melting of the lithospheric mantle. Geochimica et Cosmochimica Acta 60, 423-437.
870 Chazot, G., Lowry, D., Menzies, M., Mattey, D., 1997. Oxygen isotopic composition of hydrous and anhydrous
871 mantle peridotites. Geochimica et Cosmochimica Acta 61, 161-169.
872 Cottin, J.Y., Lorand, J.P., Agrinier, P., Bodinier, J.L., Liégeois, J.P., 1998. Isotopic (O, Sr, Nd) and trace element
873 geochemistry of the Laouni layered intrusions (Pan-African belt, Hoggar, Algeria): evidence for post-
874 collisional continental tholeiitic magmas variably contaminated by continental crust. Lithos 45, 197-222.
875 Dautria, J.M., Liotard, J.M., Bosch, D., Alard, O., 2010. 160 Ma of sporadic basaltic activity on the Languedoc
876 volcanic line (Southen France): A peculiar case of lithosphere-asthenosphere interplay. Lithos 120, 202-
877 222.
878 Downes, H., Reichow, M.K., Mason, P.R.D., Beard, A.D., Thirlwall, M.F., 2003. Mantle domains in the
879 lithosphere beneath the French Massif Central: trace element and isotopic evidence from mantle
880 clinopyroxenes. Chemical Geology 200, 71-87.
881 Downes, H., 2007. Origin and significance of spinel and garnet pyroxenites in the shallow lithospheric
882 mantle: Ultramafic massifs in orogenic belts in Western Europe and NW Africa. Lithos 99: 1-24.
883 Droop, G.T.R., 1987. A general equation for estimating Fe^{3+} concentrations in ferromagnesian silicates and
884 oxides from microprobe analyses, using stoichiometric criteria. Mineralogical Magazine 51, 431-435.
885 El Azzouzi, M., Bernard- Griffiths, J., Bellon, H., Maury, R. C., Piqué, A., Fourcade, S., Cotten, J., Hernandez, J.,
886 1999. Evolution des sources du volcanisme marocain au cours du Néogène. Comptes Rendus de
887 l'Académie des Sciences de Paris, Sciences de la Terre et des Planètes 329, 95-102.

El Azzouzi, M., Maury, R., Bellon, H., Youbi, N., Cotten, J., Kharbouch, F., 2010. Petrology and K-Ar chronology of the Neogene-Quaternary Middle Atlas basaltic province Morocco. Bulletin de la Société Géologique de France 181, 243-257.

Fabriès, J., Figueroa, O., Lorand, J.P., 1987. Petrology and thermal history of highly deformed mantle xenoliths from the Montferrier basanites, Languedoc, southern France: A comparison with Ultramafic Complexes from the north Pyrenean Zone. Journal of Petrology 28, 887-919.

Fabriès, J., Lorand, J.P., Bodinier, J.L., 1998. Petrogenetic evolution of orogenic lherzolite massifs in the central and western Pyrenees. Tectonophysics 292, 145-167.

Féménias, O., Coussaert, N., Bingen, B., Whitehouse, M., Mercier, J.C.C., Demaiffe, D., 2003. A Permian underplating event in the late- to post-orogenic tectonic setting. Evidence from the mafic-ultramafic layered xenoliths from Beaunit (French Massif Central). Chemical Geology 199, 293-315.

France, L., Nicollet, C., 2010. MetaRep, an extended CMAS 3D program to visualize mafic (CMAS, ACF-S, ACF-N) and politic (AFM-K, AFM-S, AKF-S) projections. Computers & Geosciences 36, 786-791. doi:10.1016/j.cageo.2010.01.001

France, L., Ouillon, N., Chazot, G., Kornprobst, J., Boivin, P., 2009. CMAS 3D a new program to rapidly visualise and project major elements compositions in the CMAS system. Computers and Geosciences 35, 1304-1310. doi:10.1016/j.cageo.2008.07.002.

France, L., Ildefonse, B., Koepke, J., Bech, F., 2010. A new method to estimate the oxidation state of basaltic series from microprobe analyses. Journal of Volcanology and Geothermal Research 189, 340-346. doi: 10.1016/j.jvolgeores.2009.11.23

France, L., Koepke, J., MacLeod, C.J., Ildefonse, B., Godard, M., Deloule, E., 2014. Contamination of MORB by anatexis of magma chamber roof rocks: constraints from a geochemical study of experimental melts and associated residues. Lithos 202-203, 120-137. doi : 10.1016/j.lithos.2014.05.018

Frey, F.A., 1980. The origin of pyroxenites and garnet pyroxenites from Salt Lake Crater, Oahu, Hawaii: trace element evidence. American Journal of Science 280-A, 427-449.

Gao, Y., Hoefs, J., Przybilla, R., Snow, J.E., 2006. A complete oxygen isotope profile through the lower oceanic crust, ODP Hole 735B. Chemical Geology 233, 217-234.

Garrido, C.J., Bodinier, J.L., Alard, O., 2000. Incompatible trace element partitioning and residence in anhydrous spinel peridotites and websterites from the Ronda orogenic peridotite. Earth and Planetary Science Letters 181, 341-358.

Gasquet, D., Levresse, G., Cheilletz, A., Azizi-Samir, M.R., Mouttaq, A., 2005. Contribution to a geodynamic reconstruction of the Anti-Atlas (Morocco) during Pan-African times with the emphasis on inversion tectonics and metallogenic activity at the Precambrian–Cambrian transition. Precambrian Research 140, 157-182.

Gasparik, T., 2014. Phase diagrams for geoscientists. An atlas of the Earth's inerior. Second ed., Springer New York. doi:10.1007/978-1-4614-5776-3.

Godard, M., Awaji, S., Hansen, H., Hellebrand, E., Brunelli, D., Johnson, K., Yamasaki, T., Maeda, J., Abratis, M., Christie, D., Kato, Y., Mariet, C., Rosner, M., 2009. Geochemistry of a long in-situ section of intrusive slow-spread oceanic lithosphere: Results from IODP Site U1309 (Atlantis Massif, 30°N Mid-Atlantic-Ridge). Earth and Planetary Science Letters 279, 110-122

Goncharov, A.G., Ionov, D.A., 2012. Redox state of deep off-craton lithospheric mantle: new data from garnet and spinel peridotites from Vitim, southern Siberia. Contributions to Mineralogy and Petrology 164-5: 731-745. doi: 10.1007/s00410-012-0767-z

Gonzaga, R.G., Lowry, D., Jacob, D.E., LeRoex, A., Schulze, D., Menzies, M.A., 2010a. Eclogites and garnet pyroxenites: Similarities and differences. Journal of Volcanology and Geothermal Research 190, 235-247.

Gonzaga, R.G., Menzies, M.A., Thirlwall, M.F., Jacob, D.E., LeRoex, A., 2010b. Eclogites and Garnet pyroxenites: Problems resolving provenance using Lu-Hf, Sm-Nd and Rb-Sr Isotope systems. Journal of Petrology 51(1-2), 513-535.

Granet, M., Wilson, M., Achauer, U., 1995. Imaging a mantle plume beneath the French Massif Central. Earth and Planetary Science Letters 136, 281-296.

Green, D.H., Ringwood, A.E., 1967. The genesis of basaltic magmas. Contributions to Mineralogy and Petrology 15, 103-190.

Gregory, R.T., Taylor, H.P., 1981. An Oxygen Isotope Profile in a Section of Cretaceous Oceanic Crust, Samail Ophiolite, Oman: Evidence for $\delta^{18}O$ Buffering of the Oceans by Deep (5 km) Seawater-Hydrothermal Circulation at Mid-Ocean. Journal of Geophysical Research 86-B4, 2737-2755.

Griffin, W.L., O'Reilly, S., 2007. Cratonic lithospheric mantle : Is anything subducted? Episodes 30(1), 43-53

Halliday, A.N., Dickin, A.P., Fallick, A.E., Fitton, J.G., 1988. Mantle dynamics: a Nd, Sr, Pb and O isotopic study of the Cameroon line volcanic chain. Journal of Petrology 29, 181-211.

Hart, S. R., Hauri, E. H., Oschmann, L. A., Whitehead J. A., 1992. Mantle plumes and entrainment: isotopic evidence. Science 256, 517-520.

948 Harte, B., Kirkley, M.B., 1997. Partitioning of trace elements between clinopyroxene and garnet: data from
949 mantle eclogites. Chemical Geology 136, 1-24.
950 Haüy, R.-J., 1822. Traité de minéralogie, 2nd éd. Bachelier et Huzard, Paris.
951 Heinonen, J.S., Luttinen, A.V., Riley, T.R., Michallik, R.M., 2013. Mixed pyroxenite-peridotite sources for mafic
952 and ultramafic dikes from the Antarctic segment of the Karoo continental flood basalt province. Lithos
953 177, 366-380.
954 Henjes-Kunst, F., Altherr, R., Baumann, A., 1990. Evolution and composition of the lithospheric mantle
955 underneath the western Arabian peninsula: constraints from Sr-Nd isotope systematics of mantle
956 xenoliths. Contributions to Mineralogy and Petrology 105, 460-472.
957 Henk, A., Franz, L., Teufel, S., Oncken, O., 1997. Magmatic underplating, extension, and crustal
958 reequilibration: Insights from a cross-section through the Ivrea zone and Strona-Ceneri Zone, Northern
959 Italy. The Journal of Geology 105, 367-377.
960 Hirschmann, M.M., Stolper, E.M., 1996. A possible role for garnet pyroxenites in the origin of the 'garnet
961 signature' in MORB. Contributions to Mineralogy and Petrology 124, 185-208.
962 Hirschmann, M.M., Kogiso, T., Baker, M.B., Stolper, E.M., 2003. Alkalic magmas generated by partial melting
963 of garnet pyroxenite. Geology 31(6), 481-484
964 Huang, X.L., Xu, Y.G., Lo, C.H., Wang, R.C., Lin, C.Y., 2007. Exsolution lamellae in a clinopyroxene megacryst
965 aggregate from Cenozoic basalt, Leizhou Peninsula, South China: petrography and chemical evolution.
966 Contributions to Mineralogy and Petrology 154, 691-705.
967 Ionov, D.A., Harmon, R.S., France-Lanord, C., Greenwood, P.B., Ashchepkov, I.V., 1994. Oxygen isotope
968 composition of garnet and spinel peridotites in the continental mantle: Evidence from the Vitim xenolith
969 suite, southern Siberia. Geochimica et Cosmochimica Acta 58, 1463-1470.
970 Johnson, K.T.M., 1994. Experimental cpx/and garnet/melt partitioning of REE and other trace elements at
971 high pressures: petrogenetic implications. Mineralogical Magazine 58A, 454–455
972 Johnson, K.T.M., Dick, H.J.B., Shimizu, N., 1990. Melting in the oceanic upper mantle; an ion microprobe study
973 of diopsides in abyssal peridotites. Journal of Geophysical Research 95, 2661-2678.
974 Juvigné, E., Bastin, B., Delibrias, G., Evin, J., Gewelt, M., Gilot, E., Streel, M., 1996. A comprehensive pollen and
975 tephra-based chronostratigraphic model for the Late-glacial and Holocene period in the French Massif-
976 Central. Quaternary International 34-36, 113-120.

977 Kaeser, B., Olker, B., Kalt, A., Altherr, R., Pettke, T., 2009. Pyroxenite xenoliths from Marsabit (Northern
978 Kenya): evidence for different magmatic events in the lithospheric mantle and interaction between
979 peridotite and pyroxenite. Contributions to Mineralogy and Petrology 157, 453-472.
980 Kamgang, P., Chazot, G., Njonfang, E., Tchoua, F., 2008. Geochemistry and geochronology of mafic rocks from
981 Bamenda Mountains (Cameroon): Source composition and crustal contamination along the Cameroon
982 Volcanic Line. C. R. Geosciences 340, 850-857.
983 Kogiso, T., Hirschmann, M.M., Frost, D.J., 2003. High-pressure partial melting of garnet pyroxenite: possible
984 mafic lithologies in the source of ocean island basalts. Earth and Planetary Science Letters 216(4), 603-
985 617
986 Kogiso, T., Hirschmann, M.M., Pertermann, M., 2004. High-pressure Partial Melting of Mafic Lithologies in
987 the Mantle. Journal of Petrology 45-12, 2407-2422.
988 Kornprobst, J., 1969. Le massif ultramafique des Beni Bouchera (Rif interne, Maroc): Etude des péridotites
989 de haute temperature et de haute pression et des pyroxenolites, à grenat ou sans grenat, qui leur sont
990 associées. Contributions to Mineralogy and Petrology 23, 283-322.
991 Krienitz, M. S., Haase, K. M., Mezger, K., Van den Bogaard, P., Thiemann, V., Shaikh-Mashail M. A., 2009.
992 Tectonic events, continental intraplate volcanism, and mantle plume activity in northern Arabia:
993 Constraints from geochemistry and Ar-Ar dating of Syrian lavas. Geochemistry, Geophysics, Geosystems
994 10, Q04008, doi:10.1029/2008GC002254.
995 Krienitz, M-S. and Haase, K.M., 2011. The evolution of the Arabian lower crust and lithospheric mantle –
996 Geochemical constraints from southern Syrian mafic and ultramafic xenoliths. Chemical Geology 280,
997 271-283.
998 Lambart, S., Laporte, D., Schiano, P., 2009. An experimental study of pyroxenite partial melts at 1 and 1.5
999 GPa: Implications for the major-element composition of Mid-Ocean Ridge Basalts. Earth and Planetary
1000 Science Letters 288, 335-347.
1001 Lasserre, M., Tempier, P., Soba, D., 1981. Pétrographie et géochronologie Rb/Sr des granites cambriens de
1002 Goutchoumi et d'Anloa (Cameroun). Bulletin de la Société Géologique de France 23, 511–514.
1003 Le Bas, M.J., Streckeisen, A.L., 1991. The IUGS systematics of igneous rocks. Journal of the Geological Society,
1004 London 148, 825-833.
1005 Le Roux, V., Bodinier, J.L., Alard, O., O'Reilly, S.Y., Griffin, W.L., 2009. Isotopic decoupling during porous melt
1006 flow: A case-study in the Lherz peridotite. Earth and Planetary Science Letters 279, 76-85.

1007 Lee, D. C., Halliday, A. N., Fitton, J. G., Poli, G., 1994. Isotopic variations with distance and time in the volcanic
1008 islands of the Cameroon line: Evidence for a mantle plume origin. Earth and Planetary Science Letters
1009 123, 119-138.
1010 Lee, D. C., Halliday, A. N., Davies, G. R., Essene, E. J., Fitton, J. G., Temdjim, R., 1996. Melt enrichment of
1011 shallow depleted mantle: A detailed petrological, trace element and isotopic study of mantle derived
1012 xenoliths and megacrysts from the Cameroon Line. Journal of Petrology 38, 415-441.
1013 Lenoir, X., Garrido, C.J., Bodinier, J.L., Dautria J.M., 2000. Contrasting domains beneath the Massif Central
1014 (France) revealed by geochemistry of peridotites xenoliths. Earth and Planetary Science Letters 181,
1015 359-375.
1016 Liang, Y., Sun, C., Yao, L., 2013. A REE-in-two-pyroxene thermometer for mafic and ultramafic rocks.
1017 Geochimica et Cosmochimica Acta 102, 246-260.
1018 Liu, T.C., Presnall, D.C., 2000. Liquidus phase relations in the system CaO-MgO-Al_2O_3-SiO_2 at 2.0GPa:
1019 applications to basalt fractionation, eclogites, and igneous Sapphirine. Journal of Petrology 41, 3-20.
1020 Marchesi, C., Garrido, C.J., Bosch, D., Bodinier, J.L., Gervilla, F., Hidas, K., 2013. Mantle refertilization by melts
1021 of crustal-derived garnet pyroxenite: Evidence from the Ronda peridotite massif, southern Spain. Earth
1022 and Planetary Science Letters 362, 66-75.
1023 Marzoli, A., Piccirillo, E.M., Renne, P.R., Bellieni, C., Iacumin, M., Nyobe, J.B., Tongwa, A.T., 2000. The
1024 Cameroon Volcanic Line Revisited: Petrogenesis of Continental Basaltic Magmas from Lithospheric and
1025 Asthenospheric Mantle Sources. Journal of Petrology 41, 87-109.
1026 Mattey, D., Lowry, D., Macpherson, C., 1994a. Oxygen isotope composition of mantle peridotite. Earth and
1027 Planetary Science Letters 128, 231-241.
1028 Mattey, D., Lowry, D., Macpherson, C., Chazot, G., 1994b. Oxygen isotope composition of mantle minerals by
1029 laser fluorination analysis: homogeneity in peridotites, heterogeneity in eclogites. Mineralogical
1030 Magazine 58A, 573-574.
1031 McCarthy, A., Müntener, O., 2015. Ancient depletion and mantle heterogeneity: Revisiting the Permian-
1032 Jurassic paradox of Alpine peridotites. Geology, doi: 10.1130/G36340.1
1033 Merle, O., Michon, L., 2001. The formation of the West European rift: a new model as exemplified by the
1034 Massif Central area. Bulletin Société Géologique de France 172, 213-221.

1035 Montanini, A., Tribuzio, R., Anczkiewicz, R., 2006. Exhumation history of a garnet pyroxenite-bearing mantle
1036 section from a continent-ocean transition (Northern Apennine ophiolites, Italy). Journal of Petrology 47-
1037 10: 1943-1971.
1038 Montanini, A., Tribuzio, R., Thirlwall, M., 2012. Garnet clinopyroxenite layers from the mantle sequences of
1039 the Northern Apennine ophiolite (Italy): Evidence for recycling of crustal material. Earth and Planetary
1040 Science Letters 351-352, 171-181
1041 Moore, A., 1968. Rutile exsolution in Orthopyroxene. Contributions to Mineralogy and Petrology 17, 233-
1042 236.
1043 Müntener, O., 1997. The Malenco peridotites (Alps). Petrology and geochemistry of subcontinental mantle
1044 and Jurassic exhumation during rifting Ph.D. Thesis, ETH Zürich.
1045 Natali, C., Beccaluva, L., Bianchini, G., Ellam, R.M., Siena, F. and Stuart, F.M., 2013. Carbonated alkali-silicate
1046 metasomatism in the North Africa lithosphere: Evidence from Middle Atlas spinel-lherzolites, Morocco.
1047 Journal of African Earth Sciences 41, 113-121.
1048 Nehlig, P., Boivin, P., de Herve A.D.G., Mergoil, J., Prouteau, G., Thiéblemont D., 2001. Les volcans du Massif
1049 Central. Géologues 130-131, 66-91.
1050 Nimis, P., Grütter, H., 2010. Internally consistent geothermometers for garnet peridotites and pyroxenites.
1051 Contributions to Mineralogy and Petrology 159, 411-427. doi: 10.1007/s00410-009-04555-9.
1052 O'Hara, M.J., 1967. Mineral facies in ultrabasic rocks. In: Ultramafic and related rocks, P.J. Wyllie ed., 7-18.
1053 O'Hara, M.J., Yoder, H.S.Jr., 1967. Formation and fractionation of basic magmas at high pressure. Scott. J.
1054 Geol. 3, 67-117.
1055 Pearson, D.G., Davies, G.R., Nixon, P.H., 1993. Geochemical Constraints on the petrogenesis of the diamond
1056 facies pyroxénites from the Beni Bousera peridotite massif, north Morocco. Journal of Petrology 34, 125-
1057 172.
1058 Pearson, D.G., Canil, D., Shirey, S.B., 2005. Mantle samples included in volcanic rocks: xenoliths and
1059 diamonds. In: Carlson, R.W. (Ed.), The Mantle and Core, vol. 2. Elsevier, pp. 171–275
1060 Perinelli, C., Armienti, P., Dallai, L., 2011. Thermal evolution of the lithosphere in a rift environment as
1061 inferred from the geochemistry of mantle cumulates, Northern Victoria Land, Antarctica. Journal of
1062 Petrology 52-4: 665-690.

1063 Pertermann, M., Hirschmann, M.M., 2003. Partial melting experiments on a MORB-like pyroxenite between 2
1064 and 3 GPa: constraints on the presence of pyroxenite in basalt source regions from solidus location and
1065 melting rate. Journal of Geophysical Research 108 (B2), 2125. doi:10.1029/2000JB000118.
1066 Pezzali, I., France, L., Chazot, G., Vannucci, R., 2015. Analogues of exhumed pyroxenite layers in the Alboran
1067 domain sampled as xenoliths by Middle Atlas Cenozoic volcanism. Lithos.
1068 doi:10.1016/j.lithos.2015.02.024
1069 Pilet, S., Baker, M.B., Stolper, E.M., 2008. Metasomatized Lithosphere and the Origin of Alkaline Lavas.
1070 Science 320(5878), 916-919
1071 Pique A., Michard, A., 1989. Moroccan Hercynides; a synopsis; the Paleozoic sedimentary and tectonic
1072 evolution at the northern margin of West Africa. American Journal of Science 289, 286-330.
1073 Raffone, N., Chazot, G., Pin, C., Vannucci, R., Zanneti, A., 2009. Metasomatism in the Lithospheric Mantle
1074 beneath Middle Atlas (Morocco) and the Origin of Fe- and Mg-rich Wehrlites. Journal of Petrology 50,
1075 197-249.
1076 Rankenburg, K., Lassiter, J.C., Brey, G., 2005. The role of continental crust and lithospheric mantle in the
1077 genesis of Cameroon Volcanic Line lavas: constraints from isotopic variations in lavas and megacrysts
1078 from the Biu and Jos plateaux. Journal of Petrology 46, 169-190.
1079 Rubin, K.H., Sinton, J.M., 2007. Inferences on mid-ocean ridge thermal and magmatic structure from MORB
1080 compositions. Earth and Planetary Science Letters 260: 257-276. doi: 10.1016/j.epsl.2007.05.035
1081 Seranne, M., 1999. The Gulf of Lion continental margin (NW Mediterranean) revisited by IBS: an overview.
1082 In: Durand, B., Jolivet, L. Horvath, F. & Seranne, M. (eds) The Mediterranean Basins: Tertiary Extension
1083 within the Alpine Orogen. Geological Society, London, Special Publications 156, 15-36.
1084 Shaw, J. E., Baker, J. A., Menzies, M. A., Thirlwall, M. F., Ibrahim K. M., 2003. Petrogenesis of the largest
1085 intraplate volcanic field on the Arabian Plate (Jordan): A mixed lithosphere-asthenosphere source
1086 activated by lithospheric extension. Journal of Petrology 44, 1657-1679, doi:10.1093/petrology/egg052
1087 Shaw, J. E., Baker, J. A., Kent, A.J.R., Ibrahim K. M., Menzies, M. A., 2007. The geochemistry of the Arabian
1088 lithospheric mantle-a source for intraplate volcanism? Journal of Petrology 48-8, 1495-1512,
1089 doi:10.1093/petrology/egm027
1090 Sobolev, S.V., Zeyen, H., Stoll, G., Werling, F., Altherr, R., Fuchs, K., 1996. Upper mantle temperatures from
1091 teleseismic tomography of French Massif Central including effects of composition, mineral reactions,
1092 anharmonicity, anelasticity and partial melt. Earth and Planetary Science Letters 139, 147-163.

1093 Sobolev, A. V., Hofmann, A. W., Sobolev, S. V., Nikogosian, I. K., 2005. An olivine-free mantle source of
1094 Hawaiian shield basalts. Nature 434(7033), 590-597.
1095 Stein, M., Goldstein, S.L., 1996. From plume head to continental lithosphere in the Arabian-Nubian shield.
1096 Nature 382, 773-778.
1097 Stein, M., Garfunkel, Z., Jagoutz, E., 1993. Chronothermometry of peridotitic and pyroxenitic xenoliths:
1098 Implications for the thermal evolution of the Arabian lithosphere. Geochimica et Cosmochimica Acta 57,
1099 1325-1337.
1100 Streckeisen, A.L., 1976. To each plutonic rock its proper name. Earth Sci. Rev. 12: 1-33.
1101 Takazawa, E., Frey, F.A., Shimizu, N., Obata, M., 1996. Evolution of the Horoman peridotite (Hokkaido,
1102 Japan); implications from pyroxene compositions. Chemical Geology 134, 3-26.
1103 Taylor, W.R., 1998. An experimental test of some geothermometer and geobarometer formulations for
1104 upper mantle peridotites with application to the thermobarometry of fertile lherzolites and garnet
1105 websterite. Neues Jahrbuch für Mineralogie Abhandlungen 172, 381–408.
1106 Temdjim, R., 2006. Contribution à la connaissance du manteau supérieur du Cameroun au travers de l'étude
1107 des enclaves ultrabasiques et basiques remontées par les volcans de Youkou (Adamaoua) et de Nyos
1108 (Ligne du Cameroun). Thesis, Université de Yaoundé 1 ; IRD, Yaoundé (CMR) ; Clermont-Ferrand, 423 p.
1109 Temdjim, R., Boivin, P., Chazot, G., Robin, C., Rouleau, E., 2004. L'hétérogénéité du manteau supérieur à
1110 l'aplomb du volcan de Nyos (Cameroun) révélée par les enclaves ultrabasiques. Comptes Rendus
1111 Geoscience 336, 1239-1244.
1112 Verhoogen, J., 1962. Distribution of titanium between silicates and oxides in igneous rocks. American
1113 Journal of Science 260, 211-220.
1114 Viljoen, K.S., Schulze, D.J., Quadling, A.G., 2005. Contrasting Group I and Group II eclogite xenoliths
1115 petrogenesis: Petrological, trace element and isotopic evidence from eclogite, garnet-websterite and
1116 alkremite xenoliths in the Kaalvallei kimberlite, South Africa. Journal of Petrology 46, 2059-2090.
1117 Wittig, N., Baker, J.A., Downes, H., 2006. Dating the mantle roots of young continental crust. Geology 34, 237-
1118 240. doi: 10.1130/G22135.1
1119 Wittig, N., Baker, J.A., Downes, H., 2007. U-Th-Pb and Lu-Hf isotopic constraints on the evolution of
1120 subcontinental lithospheric mantle, French Massif Central. Geochimica et Cosmochimica Acta 71, 1290-
1121 1311.

1122 Wittig, N., Pearson, D.G., Baker, J.A., Duggen, S., Hoernle, K., 2010. A major element, PGE and Re-Os isotope
1123 study of Middle Atlas (Morocco) peridotite xenoliths: Evidence for coupled introduction of metasomatic
1124 sulphides and clinopyroxene. Lithos, 115, 15-26.
1125 Workman, R.K., Hart, S. R., 2005. Major and trace element composition of the depleted MORB mantle (DMM).
1126 Earth and Planetary Science Letters 231, 53-72.
1127 Wu, C.M., Zhao, G.C., 2012. Reply to comment on "The applicability of garnet-orthopyroxene geobarometry
1128 in mantle xenoliths" by Paolo Nimis and Herman Grütter. Lithos 142-143, 288-299
1129 Zangana, N.A., Downes, H., Thirlwall, M.F., Hegner, E., 1997. Relationship between deformation, equilibration
1130 temperatures, REE and radiogenic isotopes in mantle xenoliths (Ray Pic, Massif Central, France): an
1131 example of plume-lithosphere interaction? Contributions to Mineralogy and Petrology 127, 187-203
1132 Zheng, Y.F., 1993. Calculation of oxygen isotope fractionation in anhydrous silicate minerals. Geochimica et
1133 Cosmochimica Acta 57, 1079-1091
1134 Zhang, H.F., Mattey, D.P., Grassineau, N., Lowry, D., Brownless, M., Gurney, J.J., Menzies M.A., 2000. Recent
1135 fluid processes in the Kaapvaal Craton, South Africa: coupled oxygen isotope and trace element
1136 disequilibrium in polymict peridotites. Earth and Planetary Science Letters 176, 57-72.
1137 Zindler, A., Hart, S., 1986. Chemical geodynamics. Annual Reviews of Earth and Planetary Sciences 14, 493-
1138 571.
1139

Captions:

Figure 1: Simplified maps and sampling localities (red stars) for FMC samples (a, modified after Wittig et al., 2007), Cameroon samples (b, modified after Temdjim et al., 2004), Morocco samples (c, modified after Wittig et al., 2010), and Jordan samples (d, modified after Shaw et al., 2007).

Figure 2: Photomicrographs of the studied samples. **a)** Pl inclusion with radial fractures in the host garnet (FMC; sample LN-78; plane-polarized light); **b)** Green-Spl inclusion with radial fractures in host Grt; Grt grains are rimmed by a brown kelyphite displaying a Pl–Opx–Spl intergrowth (FMC; sample LN-78; plane-polarized light); **c)** Large Cpx porphyroclast with Opx exsolutions (FMC; sample LN-78; cross-polarized light); **d)** Small Opx–brown-Spl–Pl association at the contact of Grt+Cpx. Green-Spl inclusions are observed in Grt. Grt are rimmed by a thin brown kelyphite displaying a Pl–Opx–Spl intergrowth (FMC; sample LN-78; plane-polarized light); **e-f)** Association of Grt, Cpx, Spl, and Spr in the Morocco sample TAK-4. Grt is highly kelyphitized (brown). Spr rims the Spl grains included in Grt, and is present as inclusions in Spl grains (e: plane-polarized light; f: cross-polarized light). **g)** RGB image of a composite inclusion in a Cpx of the Morocco sample TAK-4; it is composed of Spr, Spl, Pl and Opx. Colors are: R=Si+Mg+Al, G=Si+K+Mg, B=K, (blue areas are altered and composed of zeolites); **h)** Modal image of sample YK-01 from Cameroon. Spl (blue) is rimed by Grt (pink). Grt is also exsolved from Cpx (green) megacrysts. Photomicrographs of thin section (**i**; cross-polarized light) and modal image **(j)** of YK-05 sample from Cameroon. Note the deformation of Cpx (green in (j)) grains that is highlighted by different polarization levels **(i)** and by the Opx (yellow in (j)) and Grt (pink in (j)) exsolutions. **k)** Sample JO-7b from Jordan; Cpx, Opx, green-Spl and Grt are observed, the Grt forms small white grains and

brownish kelyphite around Spl grains. **l)** Photomicrograph (cross-polarized light) of an Opx grain in sample JO-10e from Jordan; the Opx is extinct and contains rutile exsolutions in two crystallographic directions.

Figure 3: Mineral chemistry. **a)** Cpx and Opx compositions in molar proportions (Wo: wollastonite component; En: enstatite component; Fs: ferrosilite component). **b)** Grt compositions in molar proportions (Alm: almandine; Spess: spessartine; Grs: grossular; And: andradite). Open squares: Cameroon samples; filled squares: Jordan samples; open circles: French Massif-Central samples; filled circles: Morocco.

Figure 4: Chondrite-normalized (Anders and Grevesse, 1989) REE **(a, c, e)**, and trace element **(b, d, f)** spider diagrams for Cpx, and Grt (Table 3). **a-b)** Cpx from French Massif-Central and Morocco samples, **c-d)** Cpx from Cameroon and Jordan samples, **e-f)** Grt for all samples.

Figure 5: Whole rock major element and Ni composition diagrams (Table 4). In all diagrams, mineral composition fields are added. The dashed lines highlight correlations. Red star represents the composition of primitive MORB taken as one composition of possible trapped melt (MORB composition is taken from Rubin and Sinton, 2007; an average of 3092 data points from slow spreading ridges is used as those melts are less affected by the various processes that may occur at crustal levels in fast spreading settings, e.g., France et al., 2014); composition (in wt %) is SiO_2=50.77; TiO_2=1.38; Al_2O_3=15.37; FeO_T=9.60; MgO=7.79; CaO=11.71; Na_2O=2.45; K_2O=0.19; P_2O_5=0.15. Green star represents the composition of primitive alkaline basanite from Ethiopia taken as one composition of possible trapped melt (R. Pik personal communication, unpublished data); composition (in wt %) is SiO_2=43.5;

1190 TiO_2=2.6; Al_2O_3=12.5; FeO_T=11.0; MgO=10.4; CaO=11.9; Na_2O=2.5; K_2O=1.0; P_2O_5=0.5.
1191 Trapped melt seems to influence the Na_2O content for some samples.
1192
1193 **Figure 6:** Chondrite-normalized (Anders and Grevesse, 1989) REE **(a, c, e)** and trace element
1194 **(b, d, f)** spider diagrams for whole-rock pyroxenites. **a-b)** French Massif-Central and
1195 Morocco samples, **c-d)** Cameroon samples, **e-f)** Jordan samples.
1196
1197 **Figure 7:** $^{143}Nd/^{144}Nd$ *versus* $^{87}Sr/^{86}Sr$ for clinopyroxene separates from Morocco, Jordan, and
1198 Cameroon. Data for DMM ($^{143}Nd/^{144}Nd$=0.51313, $^{87}Sr/^{86}Sr$=0.70263), and BSE
1199 ($^{143}Nd/^{144}Nd$=0.512638, $^{87}Sr/^{86}Sr$=0.7045) are from Workman and Hart (2005), and for HIMU
1200 ($^{143}Nd/^{144}Nd$=0.51285, $^{87}Sr/^{86}Sr$=0.70285) from Hart et al. (1992). Data are compared to
1201 regional mantle compositions (i.e., mantle xenoliths) in a), and to regional lava compositions
1202 in b). Literature data: Mantle rocks (a) from Jordan (Henjes-Kunst et al., 1990; Stein et al.,
1203 1993; Blusztajn et al., 1995; Baker et al., 1998), Morocco (Raffone et al., 2009), and
1204 Cameroon (Lee et al., 1996); and lava compositions (b) from Morocco (El Azzouzi et al.,
1205 1999), Cameroon (Halliday et al., 1988; Lee et al., 1994; Ballentine et al., 1997; Marzoli et
1206 al., 2000; Rankenburg et al., 2005; Kamgang et al., 2008), Jordan (Shaw et al., 2003; Krienitz
1207 et al., 2009).
1208
1209 **Figure 8:** Oxygen isotopic composition of the constituent minerals in the studied pyroxenites,
1210 $\delta^{18}O$ is expressed in ‰. Oxygen isotopic composition of corresponding minerals in peridotites
1211 are indicated for comparison (Ionov et al., 1994; Mattey et al., 1994a; Chazot et al., 1997;
1212 Zhang et al., 2000).
1213
1214

Figure 9: Redox conditions. Details about calculations are given in text, and values are documented in Table S1.

Figure 10: Partitioning (K_D) of trace elements between Cpx and Grt, and between Cpx and Opx. Blue dots represent results of $\mathbf{K_{D(Cpx\text{-}Grt)}}$ calculations accounting for mineral compositions using the method of Harte and Kirkley (1997). Also shown are data of Johnson (1994), Viljoen et al. (2005), Huang et al. (2007), and Raffone et al. (2009) for comparison.

Figure 11: Whole rock and Ni composition diagrams for studied pyroxenites, and various lithologies that compose oceanic crust (MORBs = 'volcanic', and the deep plutonic crust 'plutonic'). In all the diagrams, it is clear that the studied pyroxenites differ from oceanic crust lithologies. Also the Ni covariation with MgO highlights the compatible behavior of Ni during MORB differentiation (Ni decreasing with MgO), and shows that the studied pyroxenites contains higher amounts of Ni than any MORBs or even of the cumulative rocks from oceanic crust. Oceanic crust lithologies are presented using density graphs with MORB database provided by M. O'Hara (n=277), and plutonic rocks database taken from IODP Site U1309 (Godard et al., 2009; n=173).

Figure 12: P-T-t paths for the studied pyroxenites. Phase diagram for the ultramafic system is constructed after Gasparik (2014) and references therein. With increasing pressure, encountered domains are: the *plagioclase lherzolites* facies (A); the *Seiland* (B), and *Ariegites* (C) sub-facies that correspond to sub-divisions of the *spinel lherzolites* facies (B+C); and the *garnet lherzolite* facies (D). Reactions separating different facies when pressure increases are (1): Pl+Ol⇔Cpx+Opx+Spl between A and B (e.g., Takazawa et al., 1996); (2): Opx+Spl+Pl⇔Cpx+Grt between B and C (e.g., O'Hara, 1967); and (3):

Cpx+Opx+Spl⇔Ol+Grt between C and D (e.g., Johnson et al., 1990). The black line (4) is the "sapphirine reaction", namely Opx+Pl+Spl⇔Spr+Grt; it occurs only at high temperature and at slightly higher pressure than reaction (2). S is solidus. The TAK-4 path needs further constraint, the early P drop is poorly documented and a pure cooling stage is possible for this sample (dotted line).

Figure 13: Schematic evolution of the petrographic assemblage (a), and qualitative evolution of the major element (b), and trace element (c) whole rock compositions of the studied mantle cumulates. The crystallization stage corresponds to the Stage 2 in Figure 14, the metamorphism stage corresponds to the Stage 3 in Figure 14, and the metasomatism corresponds to the Stage 3' in Figure 14. In a) the initial cumulative assemblage (or magmatic assemblage from stage 2, marked 'I' in caption), is recrystallized during the subsolidus evolution (P-T-t variations) to a re-equilibrated metamorphic assemblage (marked 'II' in caption; Stage 3). Numbered circles represent the possible sampling of the cumulate by a given xenolith (theoretical samples 1-5). Xenolith '1' only samples Grt, xenolith 2 only samples Cpx, xenolith 3 only samples Opx, xenolith 4 samples a polymineralic assemblage of Cpx-Opx-Grt, xenolith 5 samples a polymineralic assemblage of Cpx-Grt. Similar sampling areas are highlighted at Stage 3 when those initial cumulative assemblages have recrystallized to metamorphic assemblages. b) and c) highlight that no modification of the whole rock composition is expected during the subsolidus evolution. Only metasomatism (Stage 3') can modify mainly the geochemical composition (enrichment in LREE and some other elements, see Section 8.3 and Table 1). In our theoretical evolution all the samples, but xenolith 3, have suffered metasomatic interactions. REE elements evolution is only qualitative, and based on minerals' Kds, and on the consideration that metasomatism is associated to LREE enrichment.

Figure 14: General schematic evolutionary model for the studied pyroxenites. At stage 1, an orogen is formed. At stage 2, the exhumation triggers a sub-isotherm decompression in the mantle, resulting in partial melting; the formed melt percolates the mantle section, and crystallizes the studied pyroxenites. After stage 2, studied pyroxenites are crystallized and their subsequent P-T-t evolution can be followed on Figure 12; their petrographical and geochemical evolution can be followed on Figure 13. Between stage 2 and 3, the exhumation is continuous until a thermal re-equilibration. After stage 3 the lithosphere is in a thermal classical regime, and contains heterogeneities (i.e., the studied pyroxenites), at that stage mantle domains can suffer metasomatism reactions (=stage 3'). Stage 4: the subsequent lithospheric evolution (thermal anomaly or rifting initiation), and with modified physical properties. In particular, the presence of pyroxenite cumulates lowers the global solidus. Compared to lherzolitic mantle regions ('un-refertilized lherzolite mantle'), partial melts will therefore occur earlier (at lower temperature), and melt production will be higher for a given temperature in such refertilized areas ('refertilized mantle').

Table 1: Sample list, region, locality, rock type, modal composition, primary magmatic paragenesis, primary magmatic facies, subsolidus paragenesis and features, facies transitions, metasomatic paragenesis or features, late features and alteration phases, microtextures, average grain size, and estimated temperatures for the studied pyroxenites. Modal proportions are given in %, *t* indicates amounts as traces. *FMC* stands for French Massif Central.

Table 2: Major element composition of minerals (in wt %). Same abbreviations as in Table 1. *n* is the number of analyses that is averaged. In the *comment* column, *Opx 1* and *Pl 1* indicate minerals observed as inclusions in Grt; *reactional* indicates minerals observed in the fine-grained Opx-Pl-Spl assemblages in FMC samples (Figure 2d). Data for *Le Pouget* sample are

from Fabriès et al. (1987). %Ph is the An content for Pl, the #Cr for Spl, and the #Mg for other phases (molar basis); %Ph2 is the jadeite content for Px, the pyrope content for Grt, and the K-feldspar content for Pl.

Table 3: Trace element concentration for minerals (ppm). Same abbreviations as in Table 1. *n* is the number of analyses that is averaged. *‘* and *“* on sample names indicates that different types of minerals are present. Underlined minerals have been analyzed at the IGG (Pavia), others at LMV (Clermont-Ferrand).

Table 4: Major (wt %) and trace (ppm) element whole rock compositions. *LN-78a* and *LN-78b* represent two different domains of sample LN-78, and *LN-78-avg* the averaged value. *bdl* means below detection limit.

Table 5: Isotopic composition of mineral separates. Same abbreviations as in Table 1. For oxygen isotope composition, some samples have been duplicated. *std err* is the standard error on the measurement.

Supplementary material:

Figure S1:

a) Oxygen isotope fractionation between Grt and Cpx. For reference, the $\Delta^{18}O=0$ line is shown (continuous line). The dashed line corresponds to fractionation at 900°C calculated using the fractionation factors of Zheng (1993). **b)** Oxygen isotope fractionation between Opx and Cpx. For reference, is shown the $\Delta^{18}O=0$ line (continuous line), and the field for lherzolites from Yemen (Chazot et al., 1997). Cpx and Grt oxygen isotopic compositions are positively correlated and plot below the line corresponding to $\Delta_{Cpx-Grt}$ = -0.4‰, indicating that these minerals have been equilibrated to T above 900° C, in agreement with T calculated using their chemical composition (see section 8.1.2.). Three samples from Cameroon (YK-01, YK-03, and YK-05) have positive $\Delta_{Cpx-Grt}$ values and record slight O-isotope disequilibrium. $\Delta_{Cpx-Opx}$ values are negative for all but two samples; the values are heterogeneous but always above $\Delta_{Cpx-Opx}$=-0.8‰.

Table S1:

Redox calculations results.

Analytical techniques

This study is based on analyses of whole rocks, and minerals that have been separated under binocular microscope for their purity after crushing, sieving and washing. In-situ analyses have been made on polished thin sections (30, 100 or 150 µm thick).

Major element mineral compositions were determined using the Cameca SX100 electron microprobe at the "Laboratoire Magmas et Volcans" (LMV) of Université Blaise-Pascal, Clermont-Ferrand, France. Instrument calibration was performed on natural standards and operating conditions were 15kV accelerating potential, 15nA beam current and 15s counting

time on peak and background. Backscattered electron (BSE) images and EDX X-ray maps were obtained on the scanning electron microscope at LMV. The modal compositions of Cameroon samples have been computed from Al, Mg, Ca, Fe mapping with the MultiSpec software (©Purdue Research Foundation, Inc. http://dynamo.ecn.purdue.edu/~biehl/MultiSpec/).

Trace element mineral compositions have been determined using a LA-ICP-MS at LMV and at the CNR-IGG of Pavia. At Pavia the LA-ICP-MS instrument couples a double focusing sector field ICP mass spectrometer (Element IR from Thermo-Finnigan) with a Q-switched Nd:YAG laser source (Quantel Brilliant) operating at 213 nm. The laser was operated at a repetition rate of 10 Hz, and the spot diameter was varied from 20 to 40 μm with a pulse energy in the range 0.01-0.03 mJ. Helium was used as the carrier gas and was mixed with Ar downstream of the ablation cell. Quantification has been done using the NIST SRM 612 glass as external standard, with 44Ca as internal standard. Precision and accuracy were assessed on the USGS BCR-2(g) reference glass and are both better than 10% for concentration at ppm level. At LMV, a Q-switched Nd-YAG laser source operating at 266 nm was coupled with a PQ2+ ICP-MS from Fisons. The laser was operated at a repetition rate of 10 Hz and the spot diameter was around 60 μm. Other analytical parameters are identical to those at Pavia laboratory and the precision and accuracy achieved are at the same level.

Whole rock major and trace element concentrations have been determined by a lithium metaborate fusion method and using an ICP-AES and an ICP-MS, respectively at the Activation Laboratories (Ontario). For sample from “Le Pouget” (FMC), the available sample amount was very small and the whole rock trace element content has been estimated using the mineral trace element compositions, and the modal proportions.

The oxygen isotopic composition of mineral separates was analyzed at the CNR-IGG of Pisa (Italy), by conventional laser fluorination, reacting the samples under a F_2 gas atmosphere.

For each sample, 1 to 2mg of separated grains were placed under a 25 W Merchantek CO_2 laser. The produced reaction triggers the oxidation of the different mineral molecules, and liberates the O_2 following reactions as $2MgO+SiO_2+xF_2 \Leftrightarrow 2MgF_2+SiF_4+2O_2+(x-4)F_2$ (with a large x in order to achieve a high total yield). The gas mixture was injected in a separation line in which different cold trap and heated salts (KCl at ~140°C) allow us to trap all the molecules but O_2. The purified O_2 is thereafter injected in a mass spectrometer (Finnigan MAT Delta plus XP) to analyze the different isotopes. A laboratory inner reference gas is jointly analyzed to compare the analyzed sample with the V-SMOW international standard. The $\delta^{18}O$ value is then calculated (with $\delta^{18}O‰ = \left(\frac{^{18}O/^{16}O_{(sample)}}{^{18}O/^{16}O_{(V-SMOW)}} - 1 \right) 1000$). The average reproducibility of oxygen isotope analyses of silicate minerals is 0.16‰. Standards were analyzed at the beginning and end of each analytical series; these were the in-house laboratory standard QMS quartz (theoretical $\delta^{18}O$ value =14.05 ‰), and UWG-2 garnet (theoretical $\delta^{18}O$ value=5.8 ‰).

The Sr-Nd radiogenic isotopic analyses have been achieved at LMV using a thermo ionization mass spectrometer (TIMS) Triton from Thermo-Finnigan. Each analysis has been accomplished on 100 mg of separate Cpx. Sr and Nd were extracted following a chromatographic extraction method after having effectuated a leaching: 30min in HCl 2.5N, 15min in HF 5%, 30min in HCl 2.5N and 30min in distilled water. Samples were then evaporated on tungsten filaments and analyzed using the double filament method with the TIMS Finnigan Triton. Standards used for this study are BIR-1 0.703136±4 and NBS987 0.710279±4 for Sr and BIR-1 0.513111±4 and AMES 0.511960±3 for Nd.

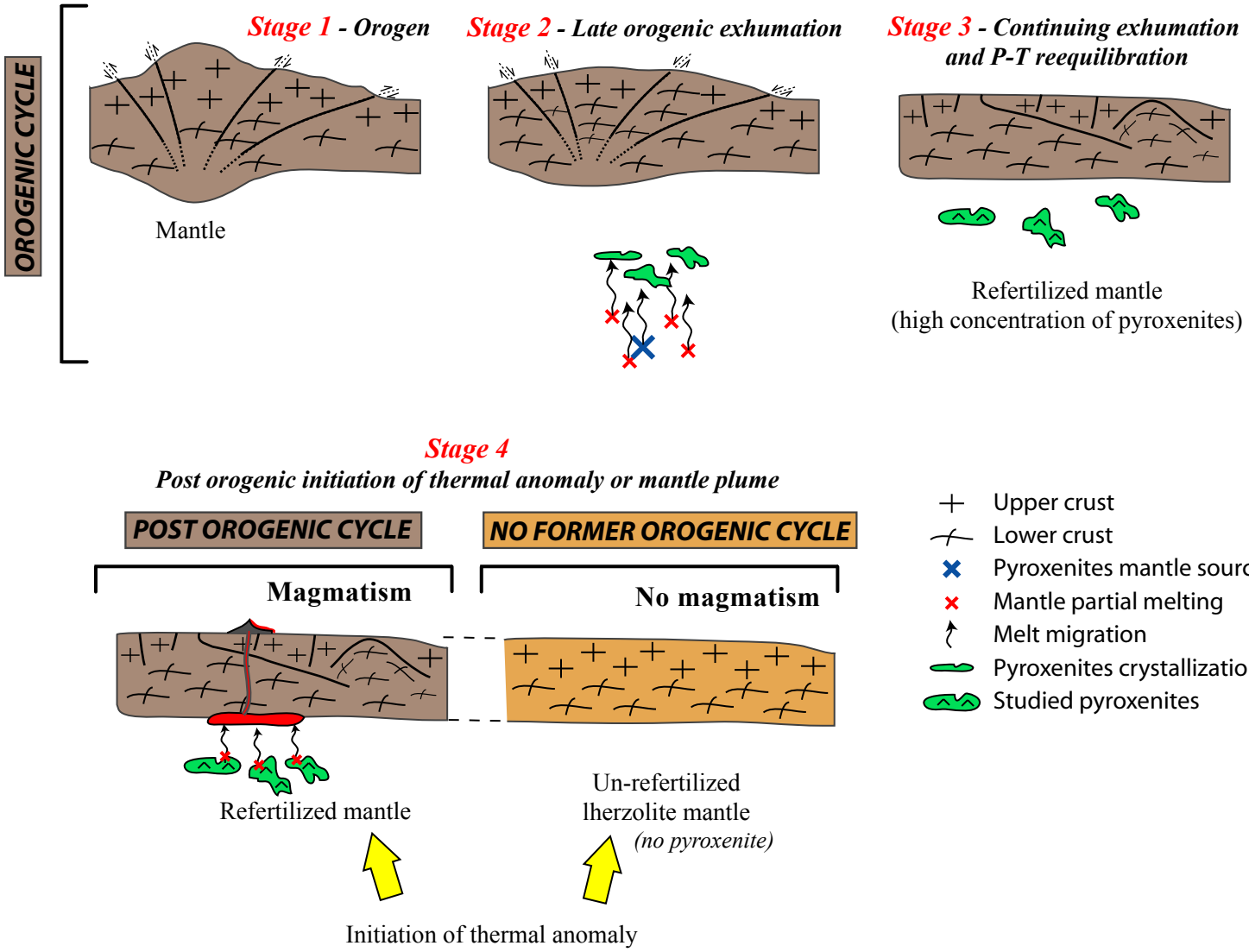
OROGENIC CYCLE
Stage 1 - Orogen
Stage 2 - Late orogenic exhumation
Stage 3 - Continuing exhumation and P-T reequilibration
Mantle
Refertilized mantle
(high concentration of pyroxenites)
Stage 4
Post orogenic initiation of thermal anomaly or mantle plume
POST OROGENIC CYCLE
NO FORMER OROGENIC CYCLE
Magmatism
No magmatism
Refertilized mantle
Un-refertilized
lherzolite mantle
(no pyroxenite)
Initiation of thermal anomaly
Upper crust
Lower crust
Pyroxenites mantle source
Mantle partial melting
Melt migration
Pyroxenites crystallization
Studied pyroxenites

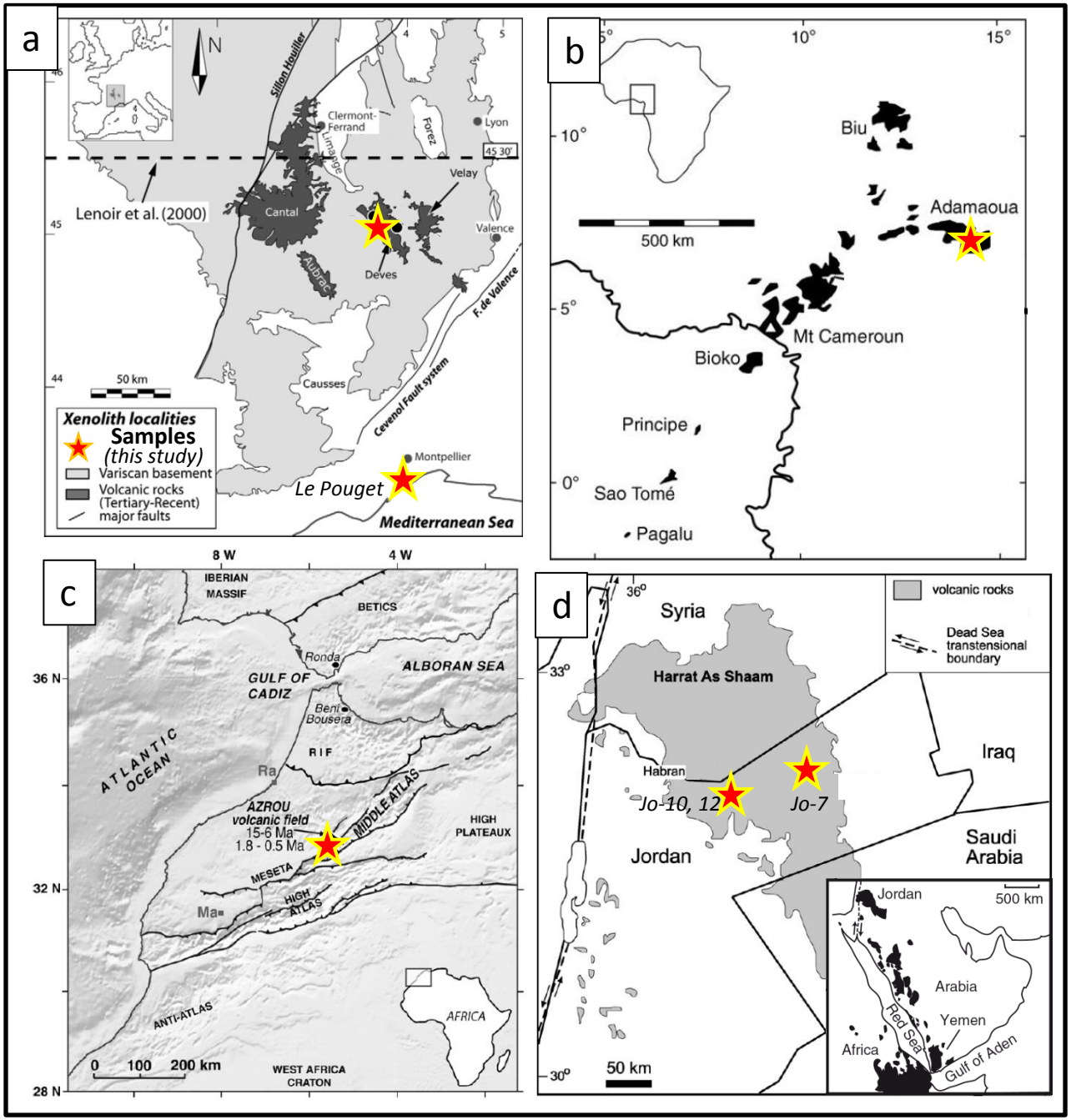

France et al., Figure 1

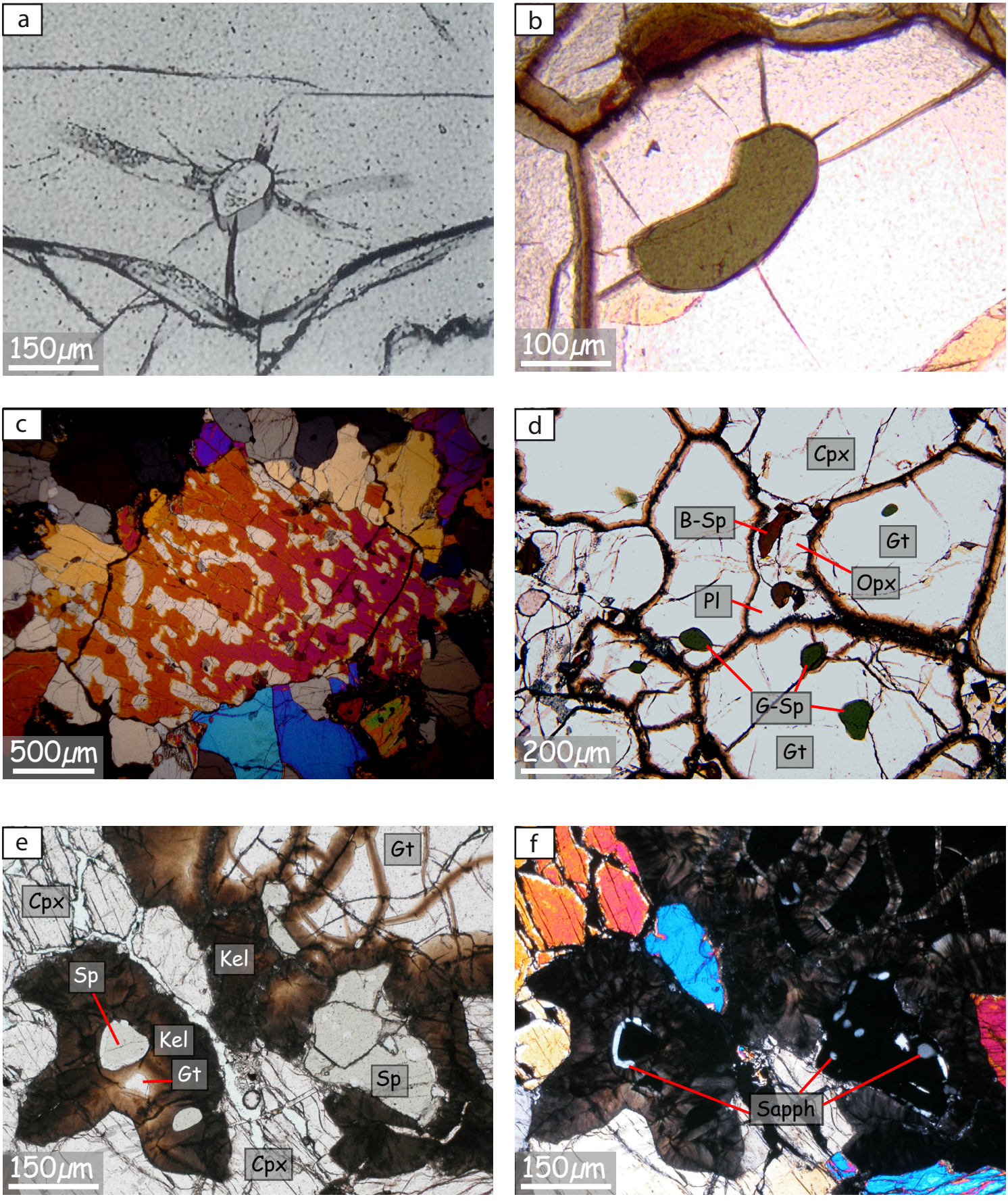

France et al., Fig. 2

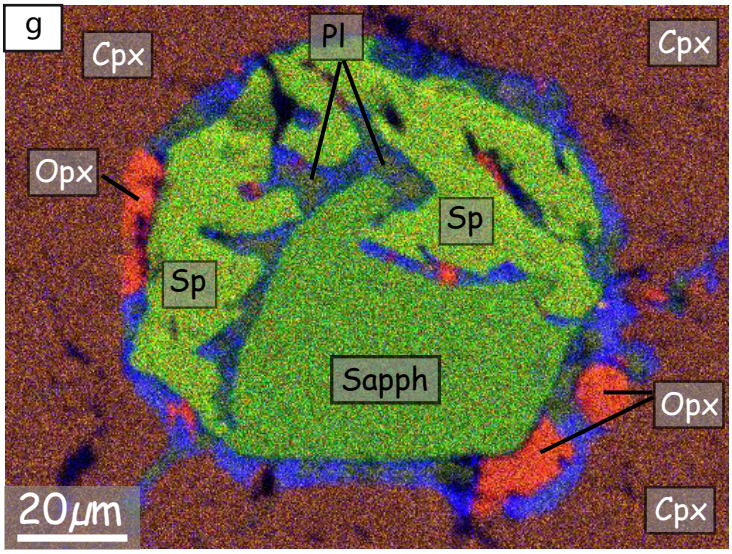

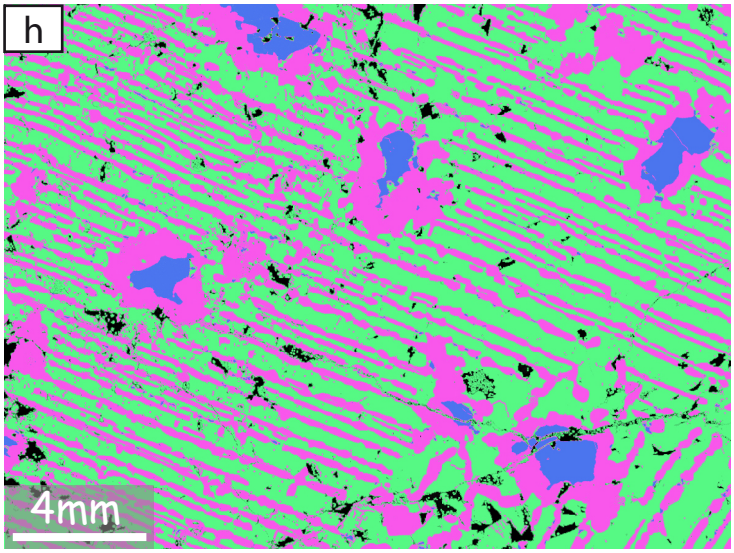

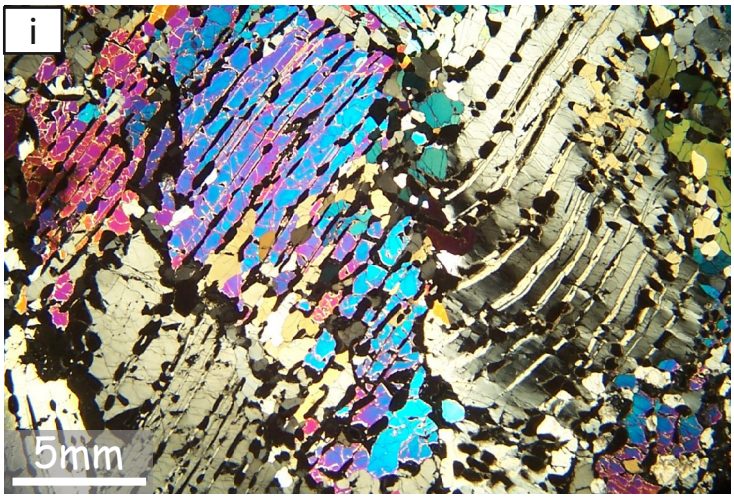

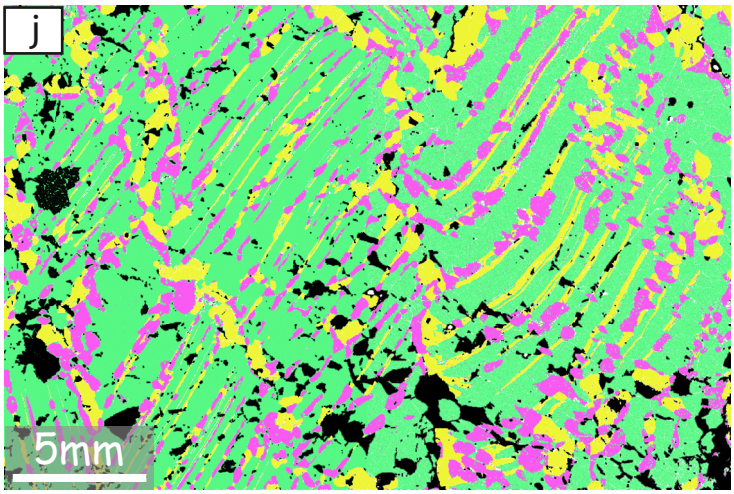

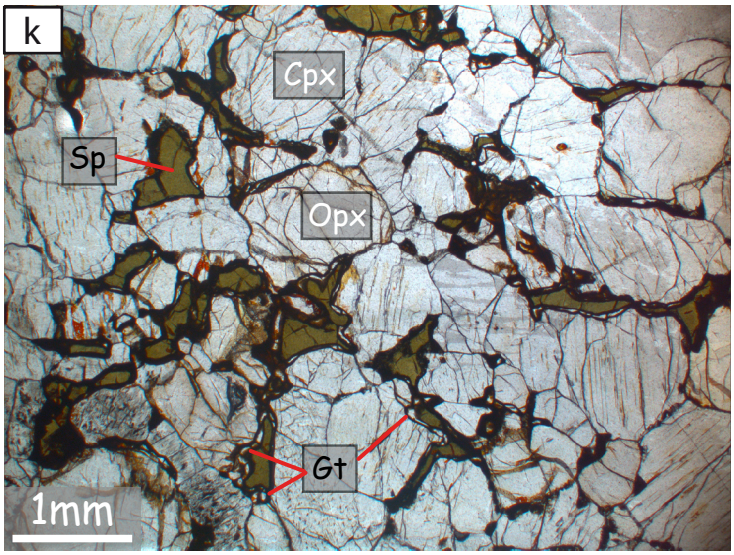

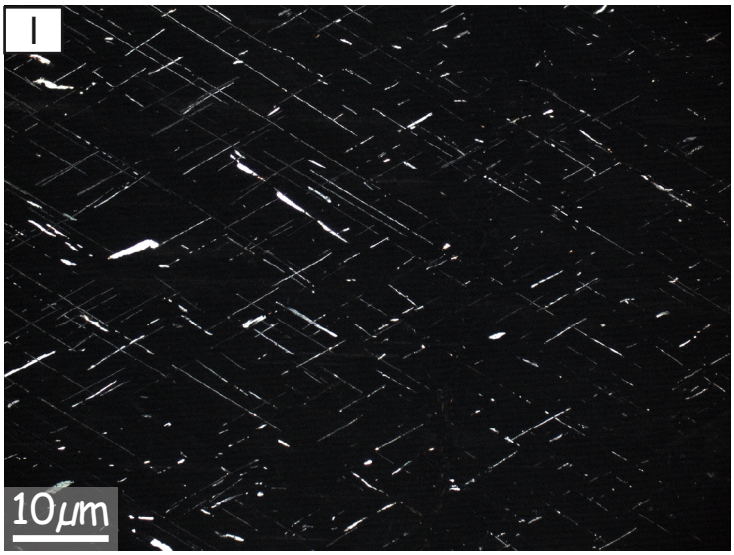

France et al., Fig. 2; continuous

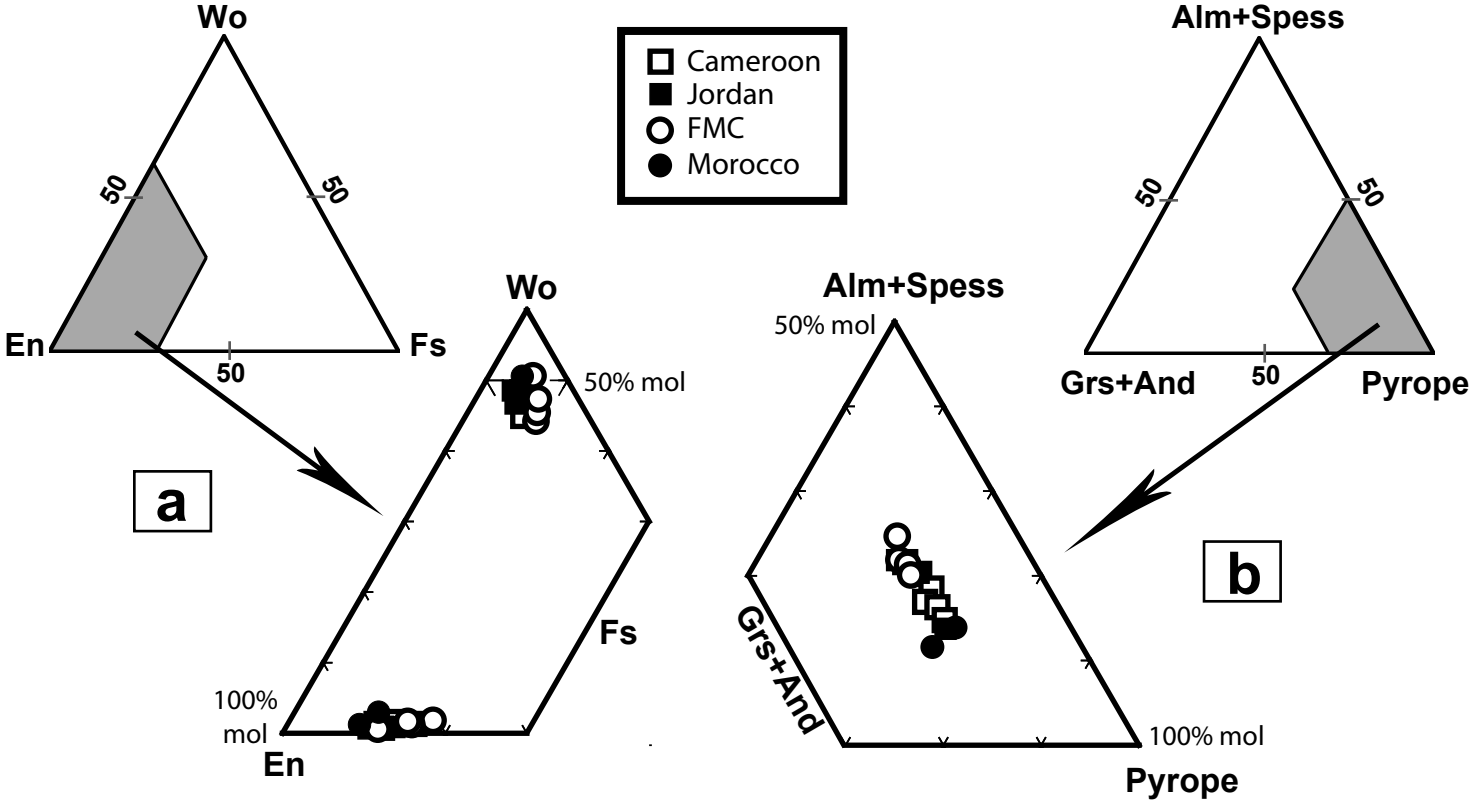

France et al., Fig. 3

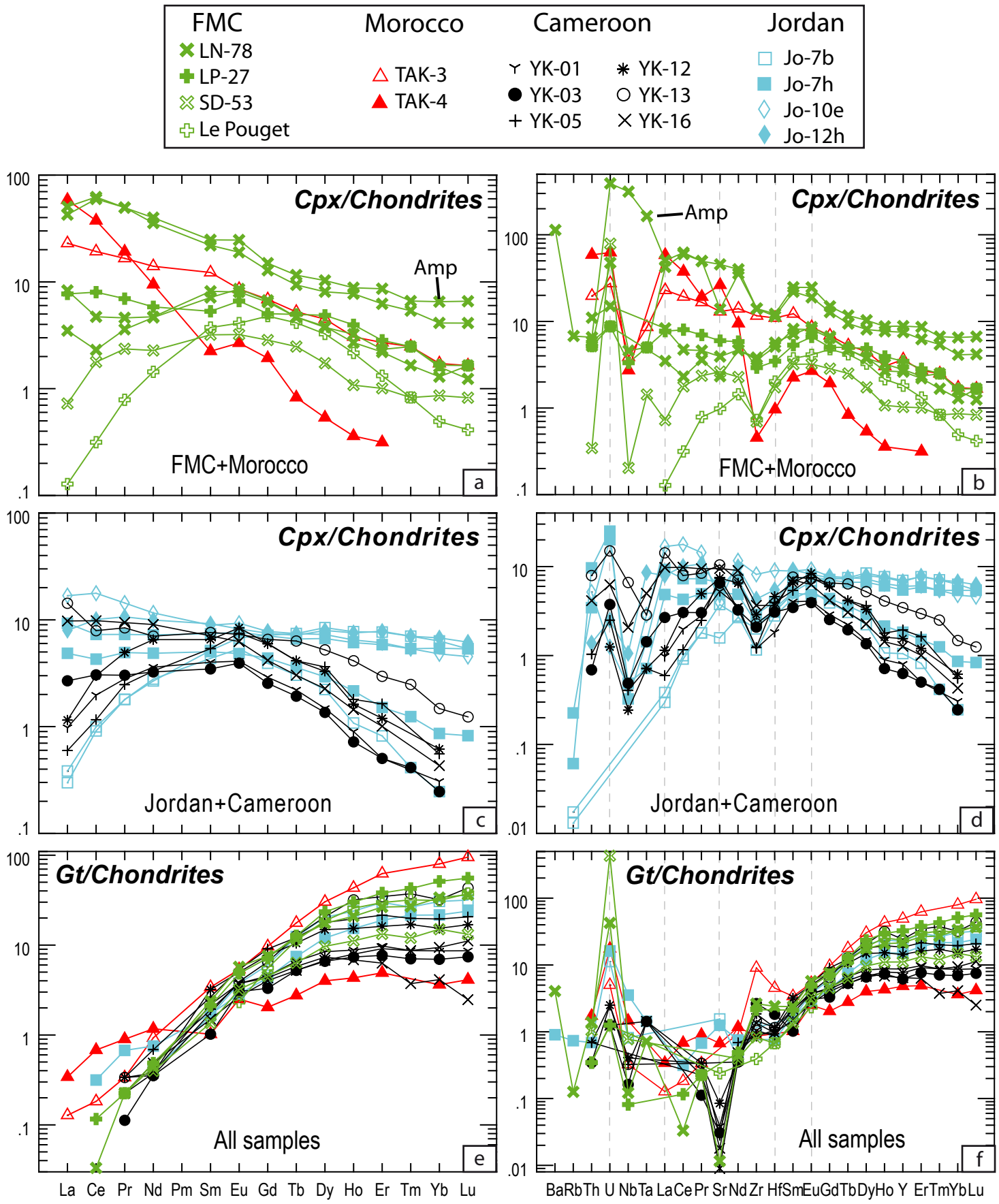

France et al., Fig. 4

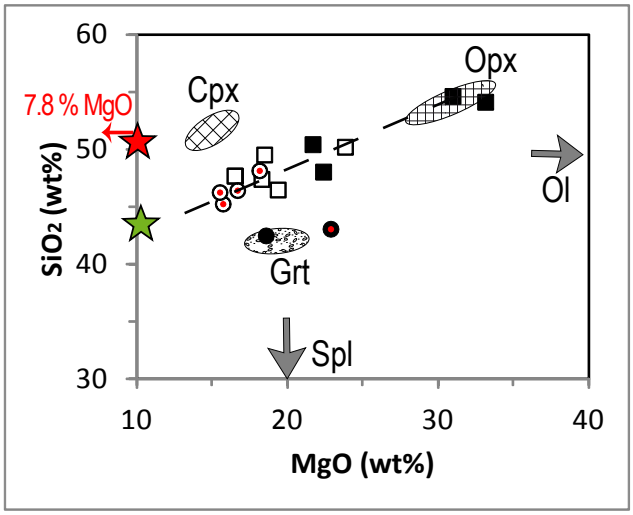

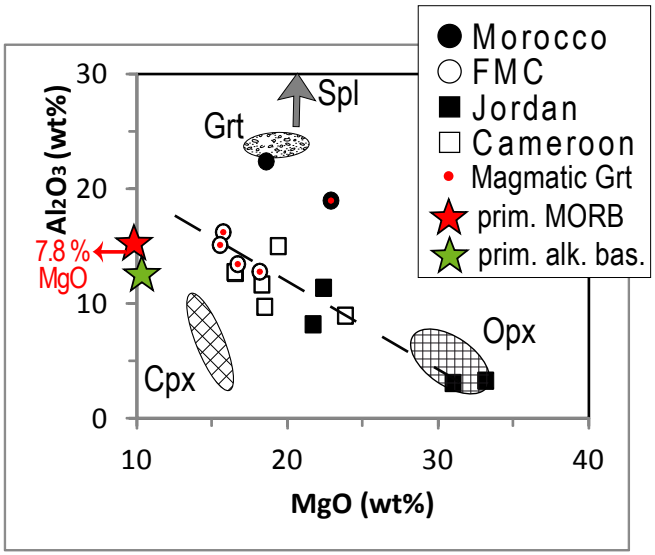

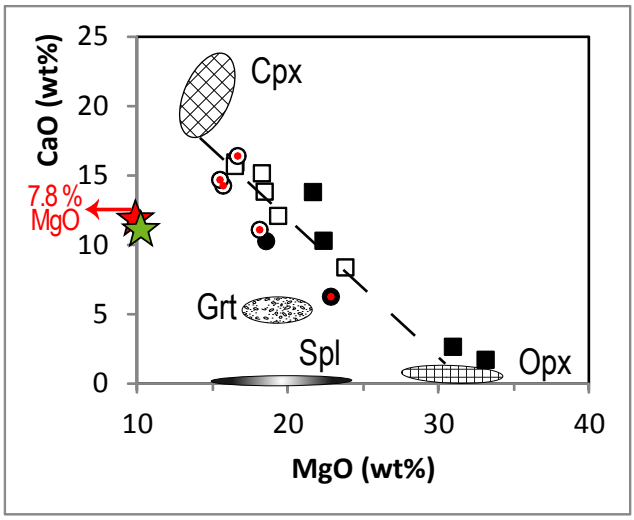

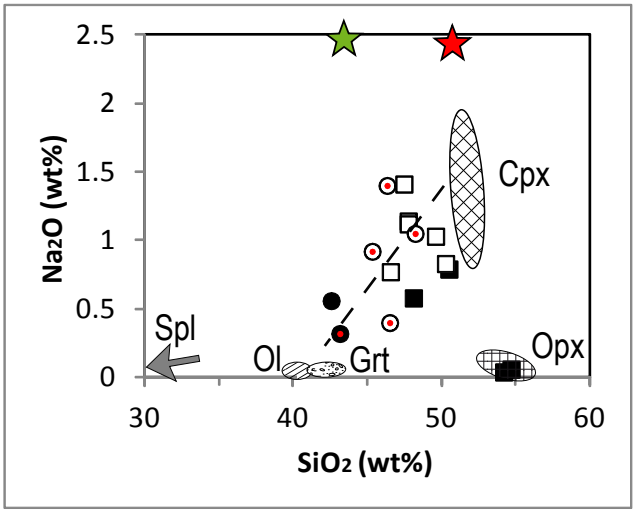

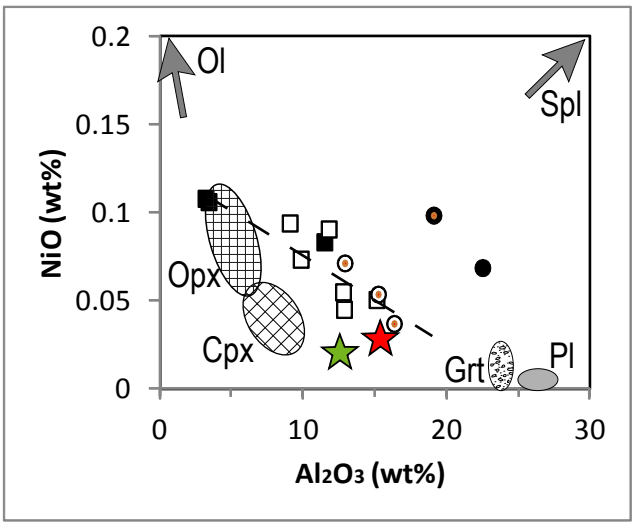

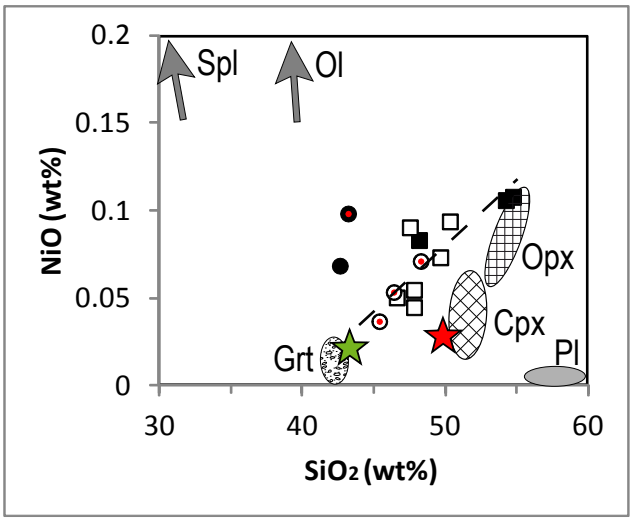

France et al., Fig. 5

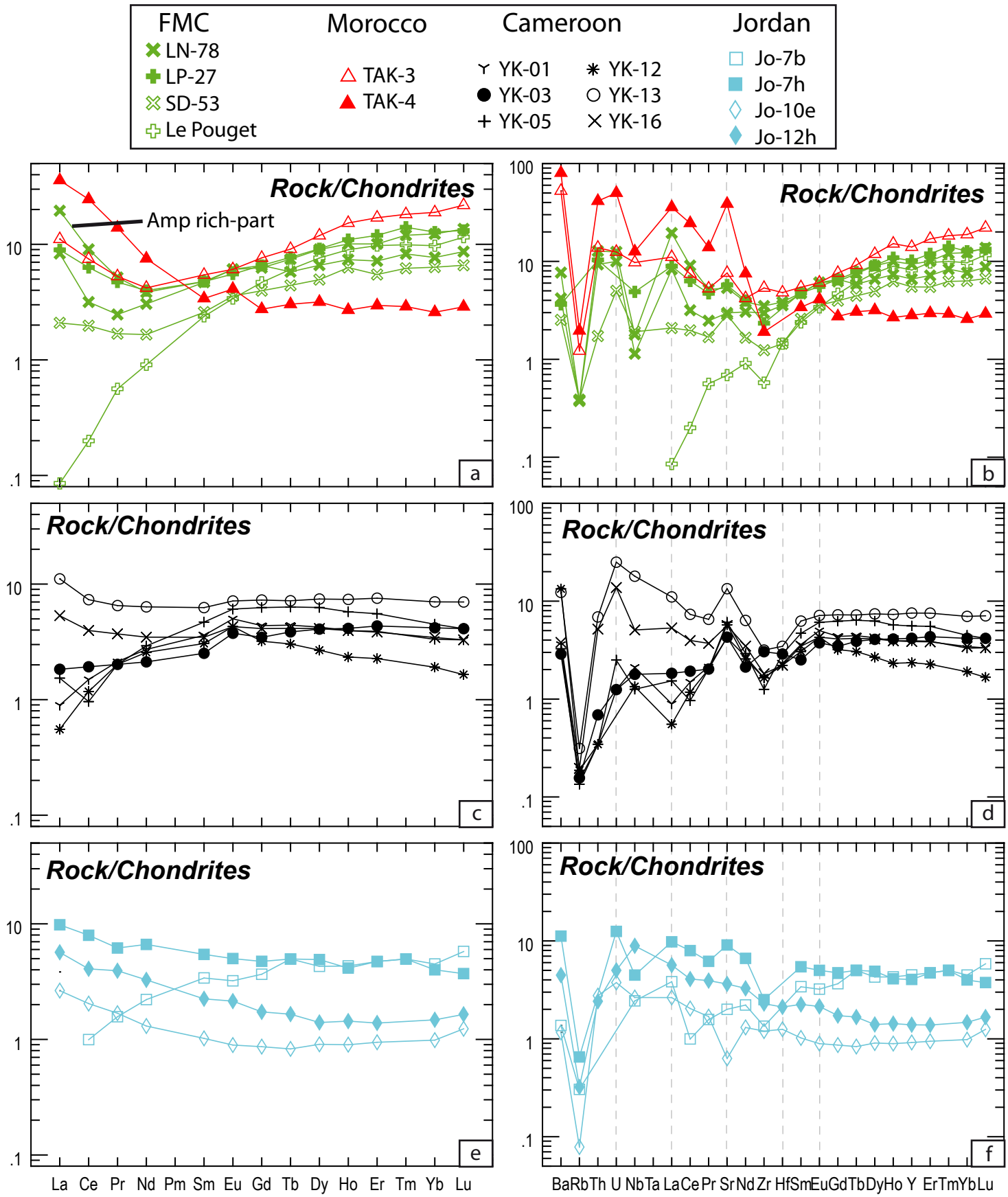

France et al., Fig. 6

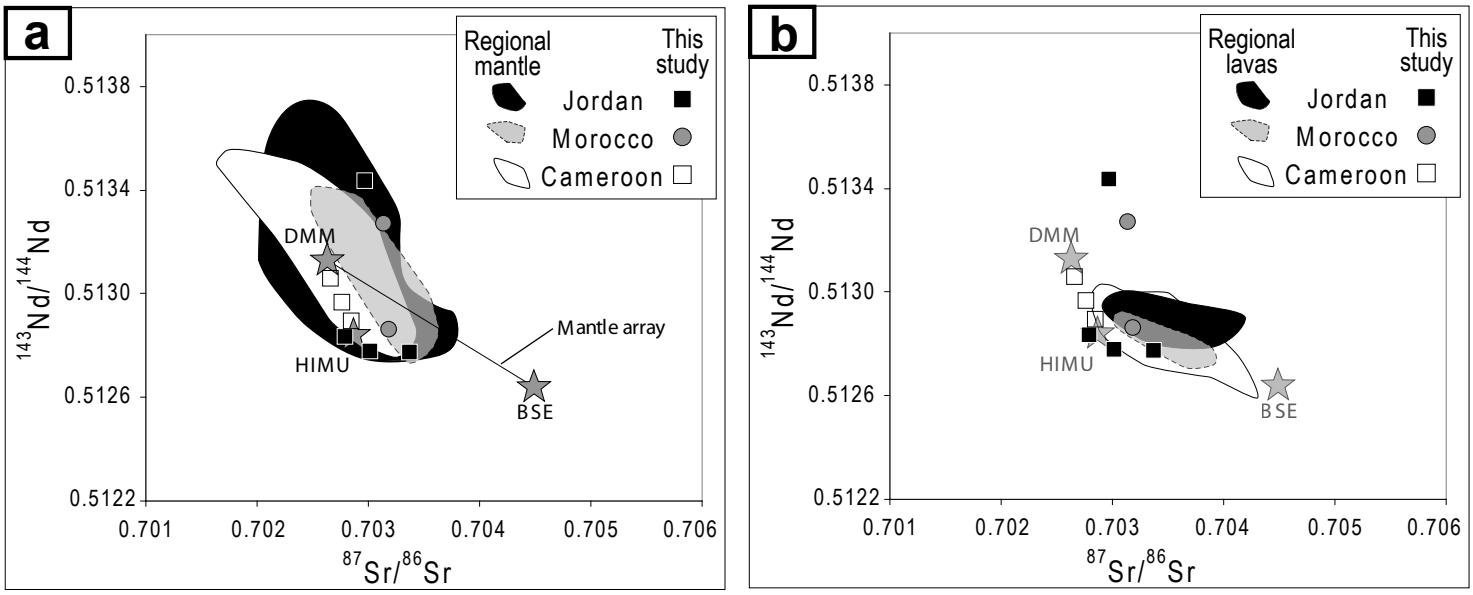

France et al., Fig. 7

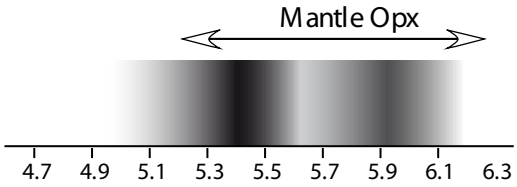

$\delta^{18}O_{Orthopyroxene}$ (‰ SMOW), *n=11*

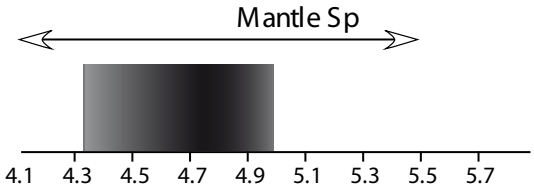

$\delta^{18}O_{Spinel}$ (‰ SMOW), *n=9*

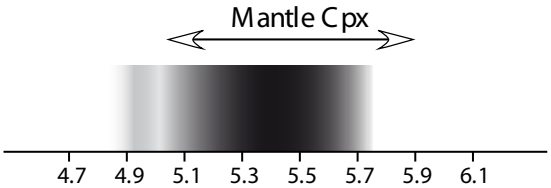

$\delta^{18}O_{Clinopyroxene}$ (‰ SMOW), *n=18*

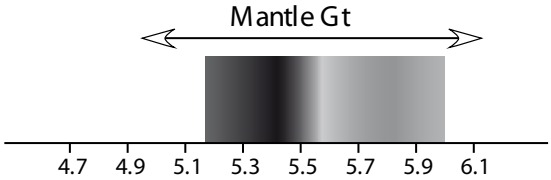

$\delta^{18}O_{Garnet}$ (‰ SMOW), *n=12*

Recycled samples (eclogites) composition: from 2 to 10 ‰

France et al., Fig. 8

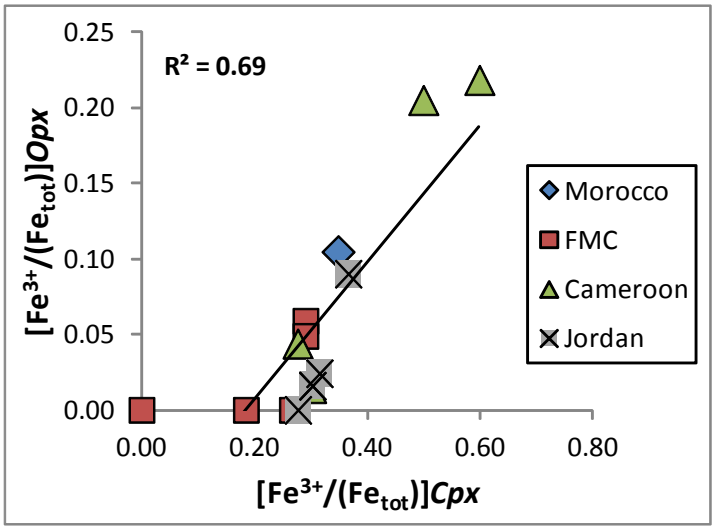

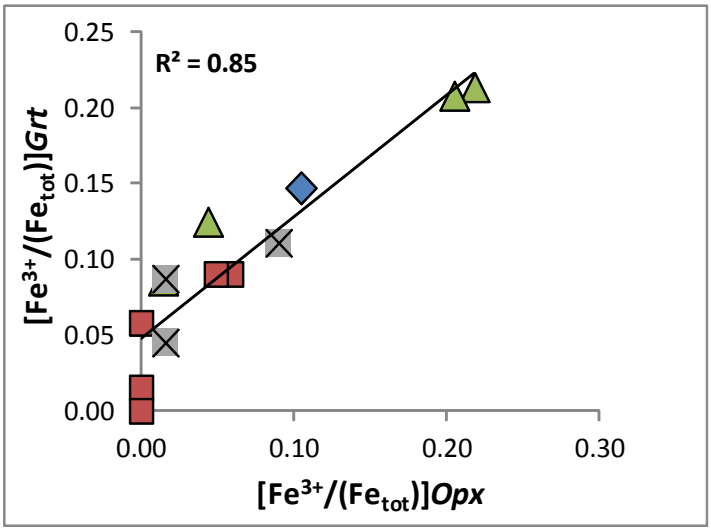

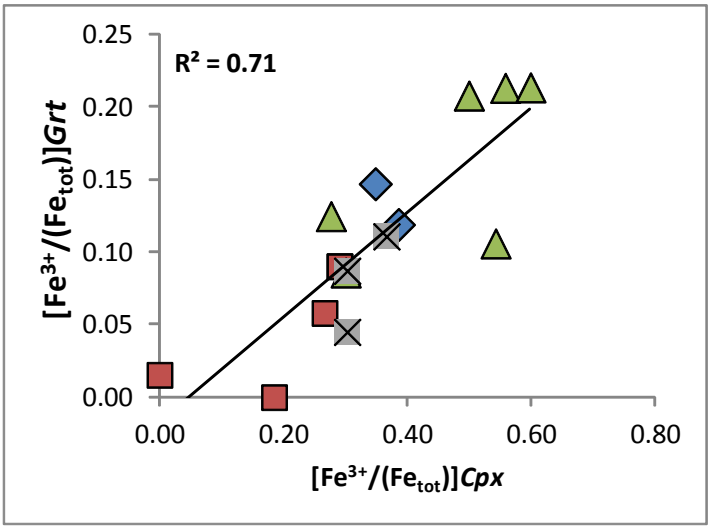

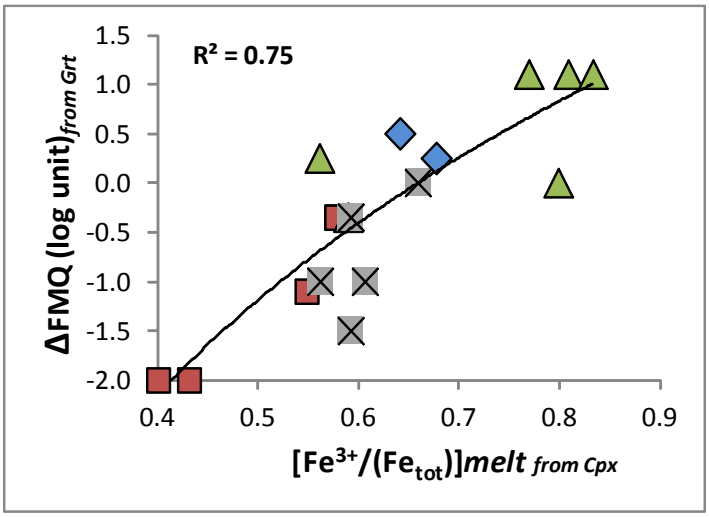

France et al., Figure 9

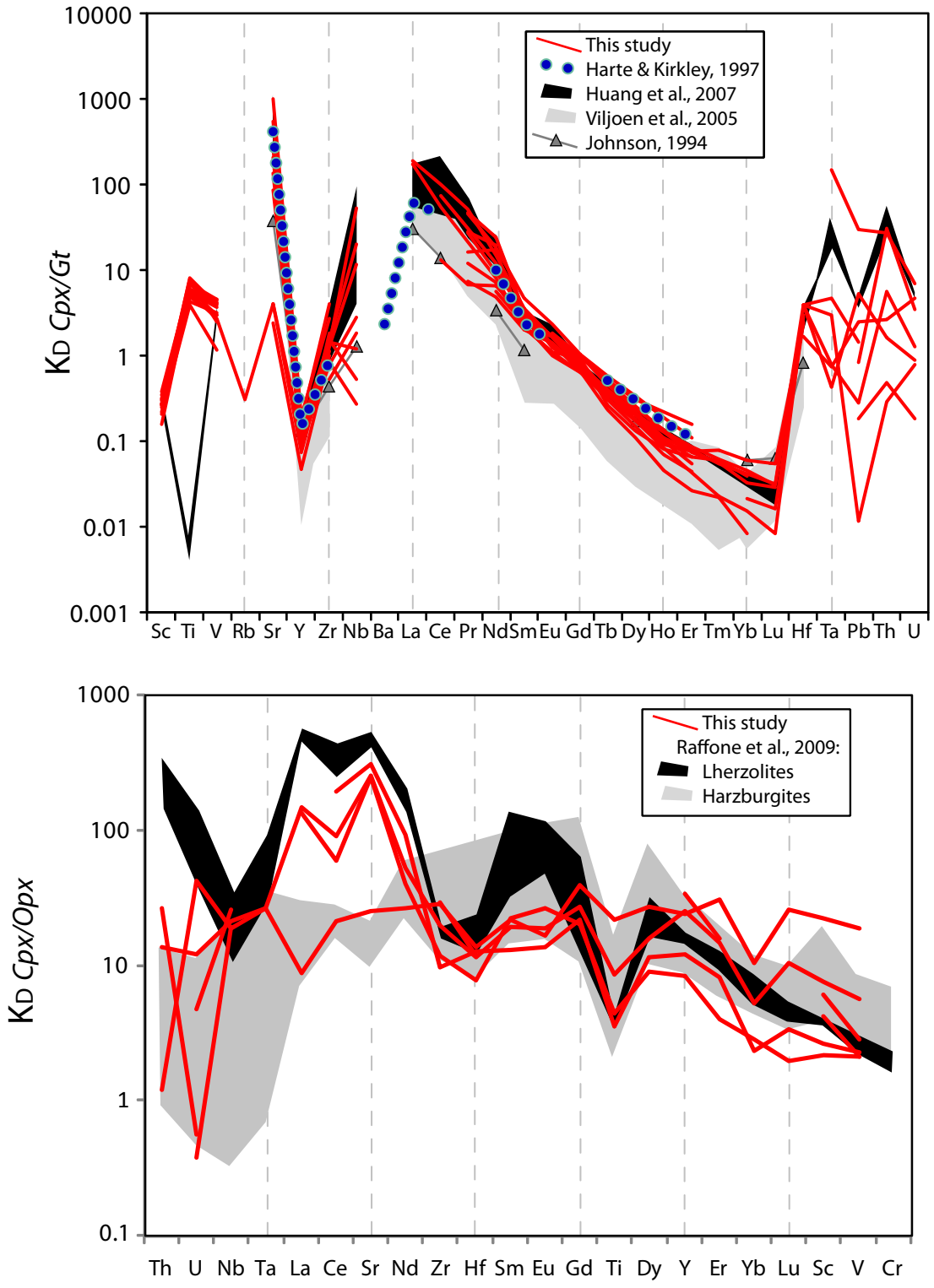

France et al., Fig. 10

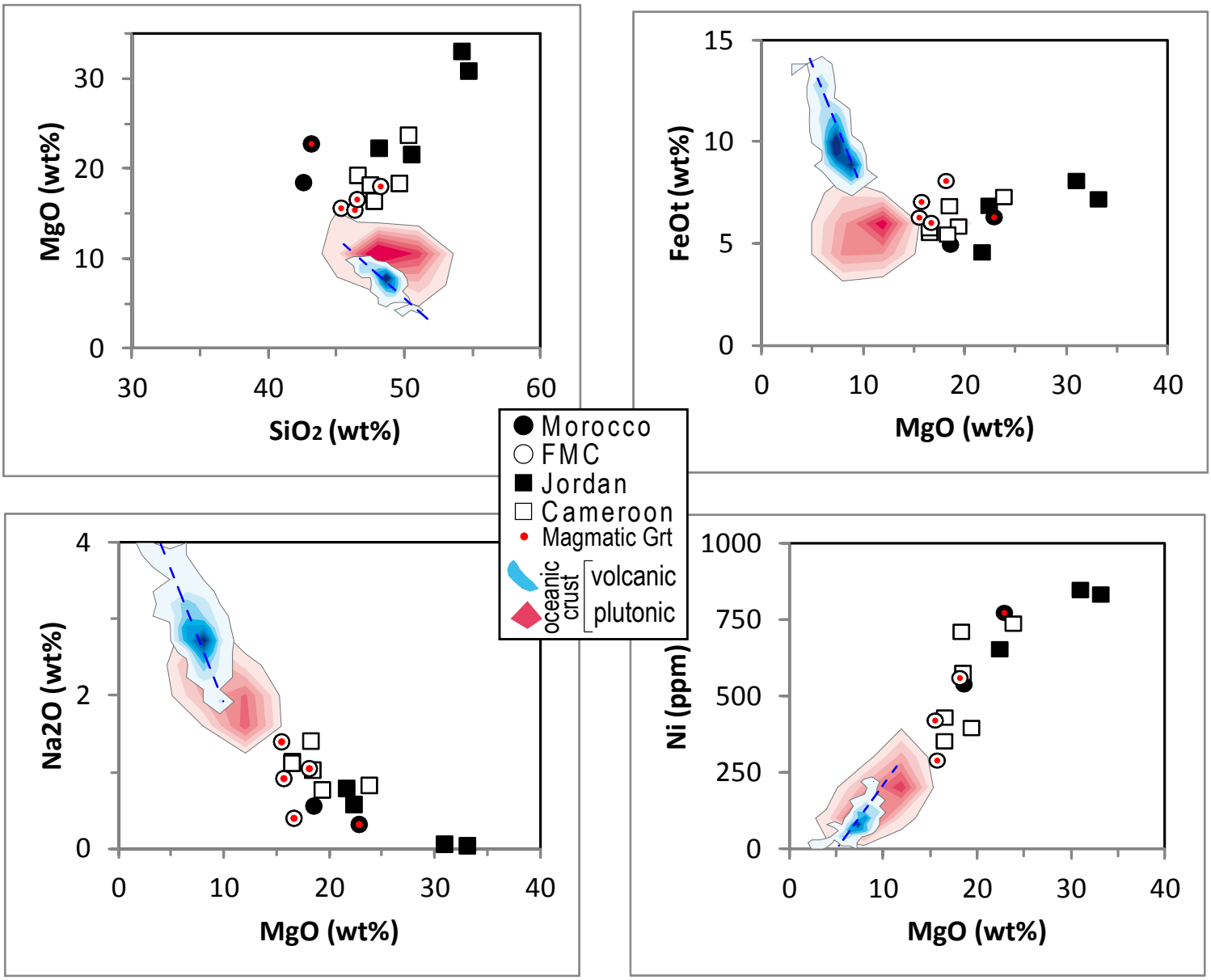

France et al., Fig. 11

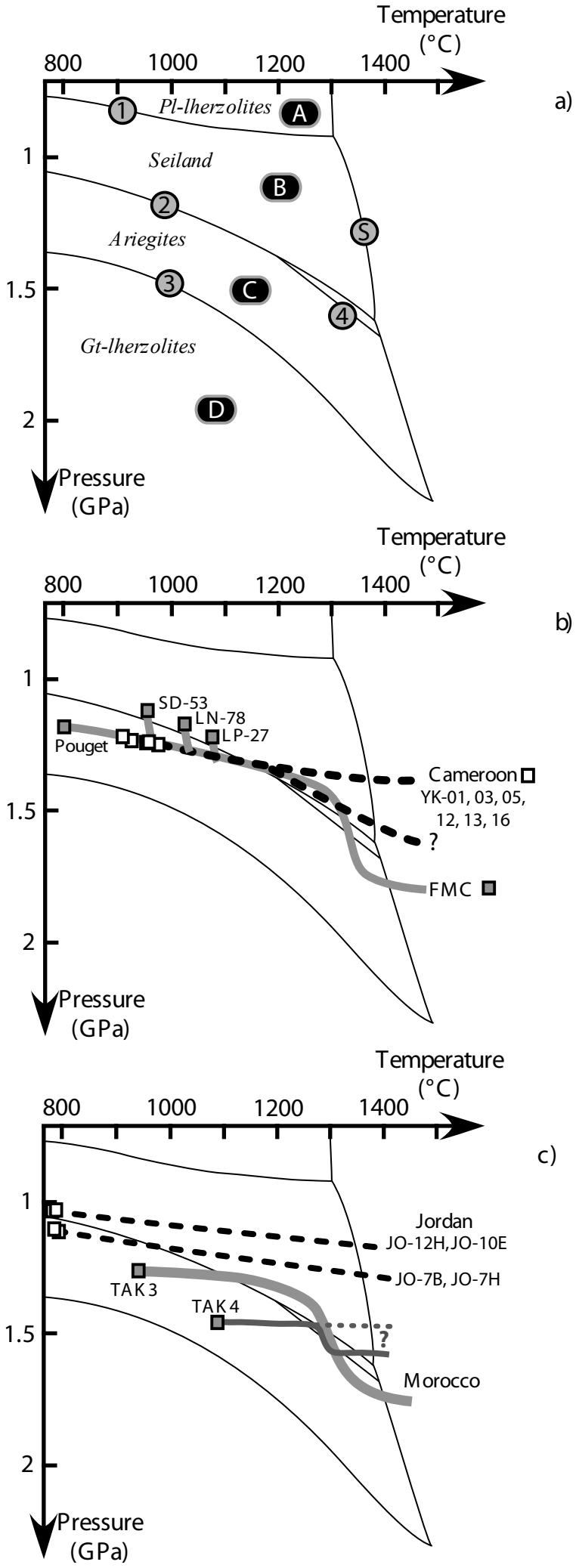

France et al., Fig. 12

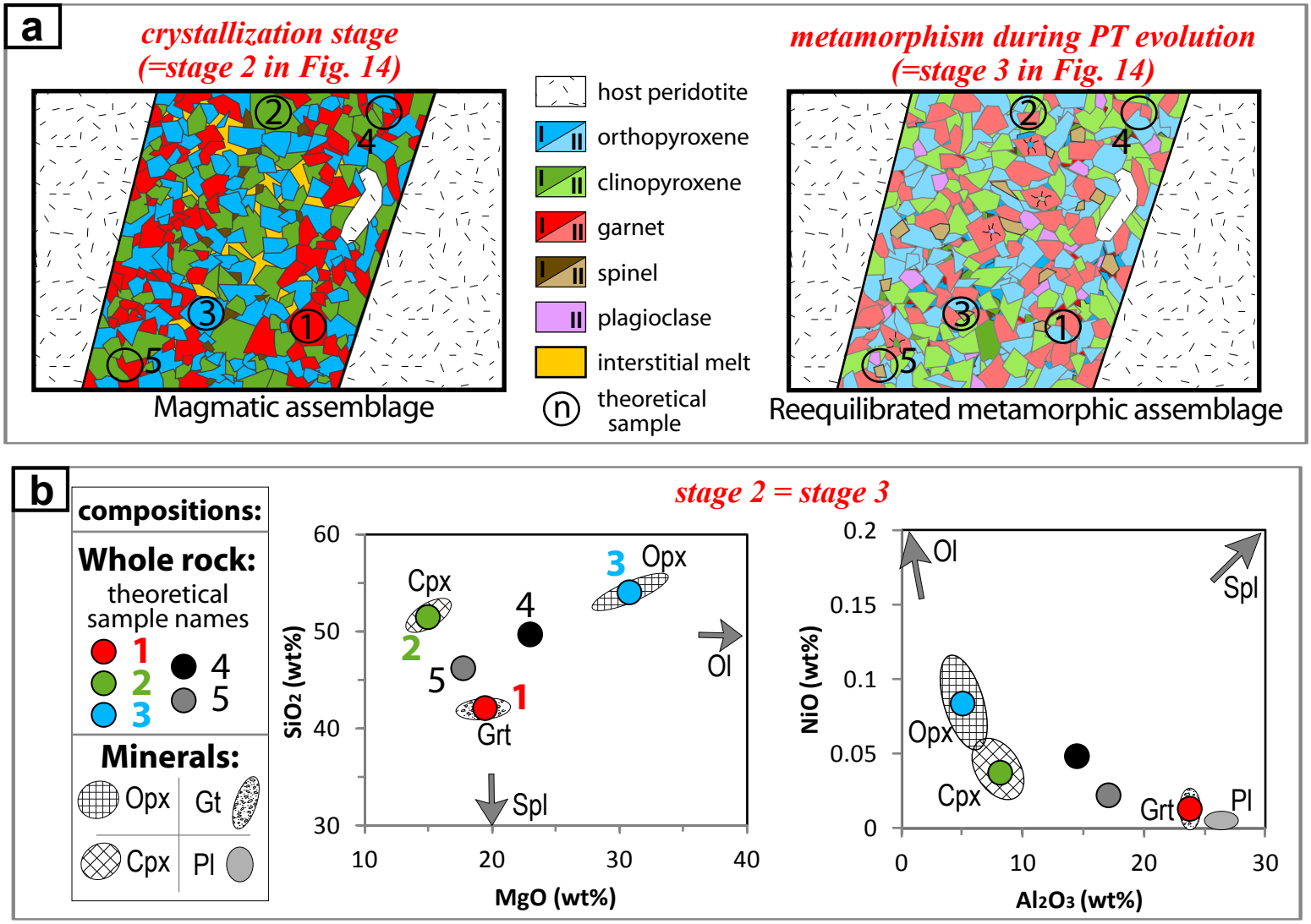

France et al., Fig. 13

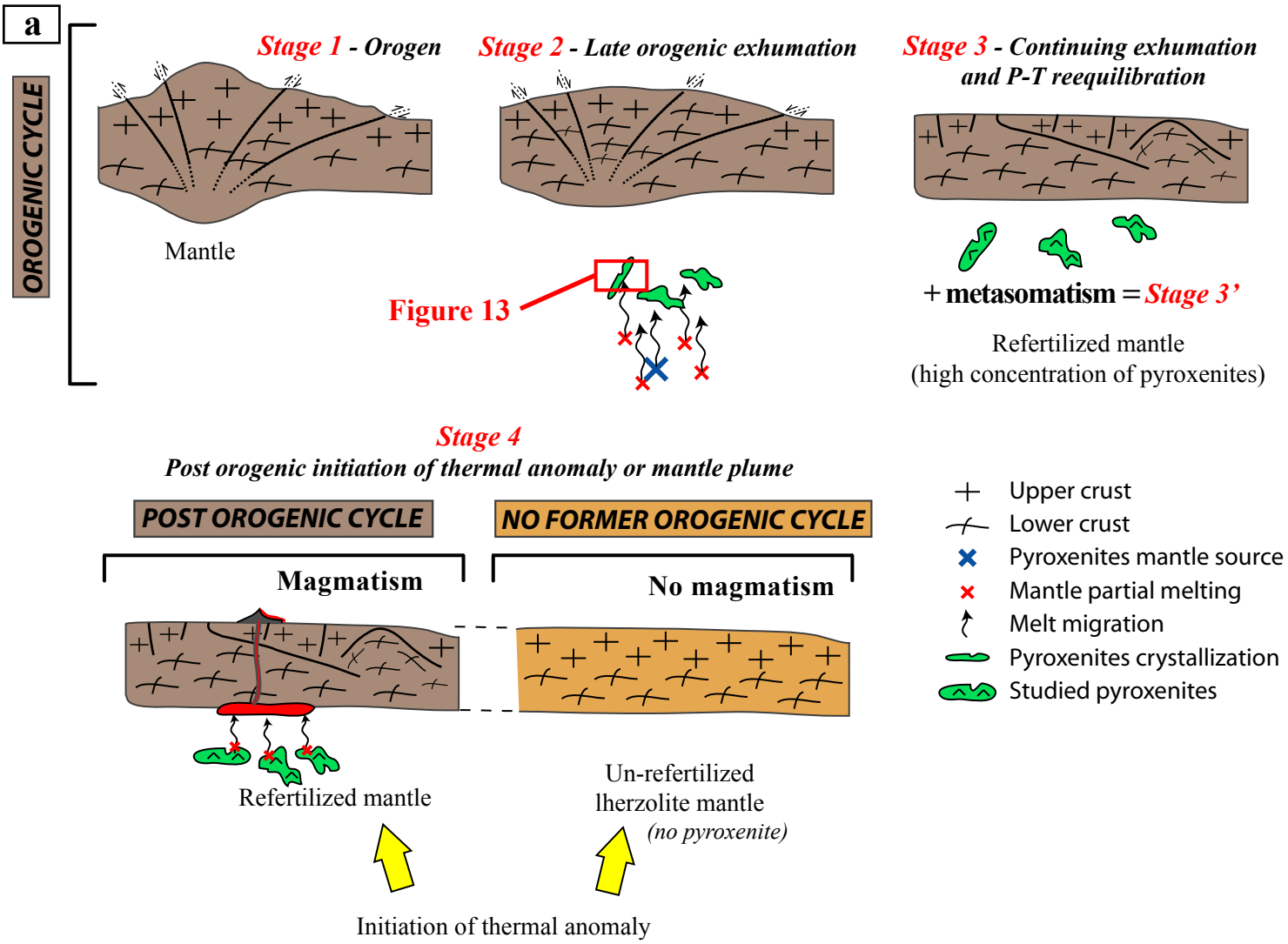
a
OROGENIC CYCLE
Stage 1 - Orogen
Stage 2 - Late orogenic exhumation
Stage 3 - Continuing exhumation and P-T reequilibration
Mantle
Figure 13
+ metasomatism = Stage 3'
Refertilized mantle
(high concentration of pyroxenites)
Stage 4
Post orogenic initiation of thermal anomaly or mantle plume
POST OROGENIC CYCLE
NO FORMER OROGENIC CYCLE
Magmatism
No magmatism
Refertilized mantle
Un-refertilized lherzolite mantle
(no pyroxenite)
Initiation of thermal anomaly
Upper crust
Lower crust
Pyroxenites mantle source
Mantle partial melting
Melt migration
Pyroxenites crystallization
Studied pyroxenites

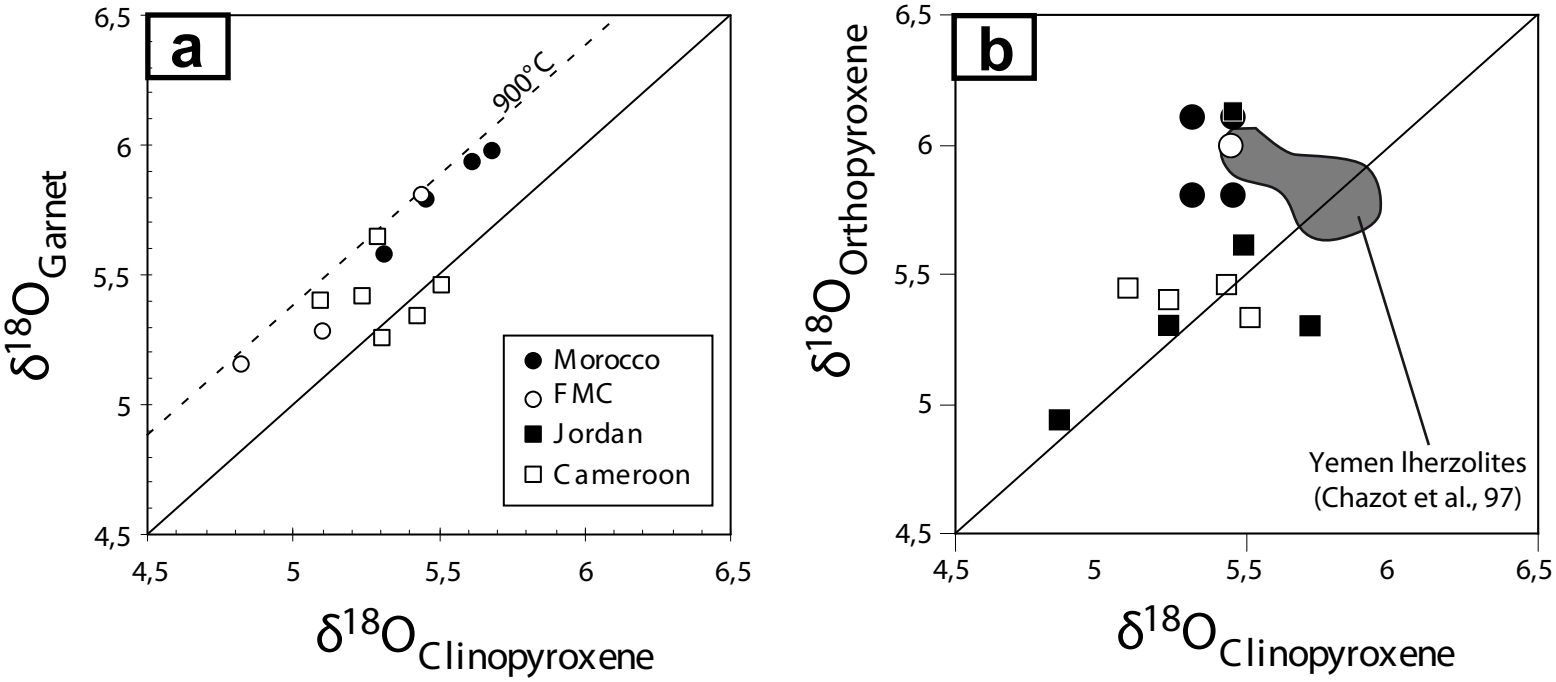

France et al., Fig. S1